Swimming and Sinking Behavior of Warm Water Pelagic Snails

Ferhat Karakas[1], Jordan Wingate[2], Leocadio Blanco-Bercial[2], Amy E. Maas[2] and David W. Murphy[1]*

[1]Department of Mechanical Engineering, University of South Florida, Tampa, FL, USA

[2]Bermuda Institute of Ocean Sciences, St. Georges, Bermuda

*** Correspondence:**
David Murphy
davidmurphy@usf.edu

Keywords: Pteropod, zooplankton, heteropod, diel vertical migration, NGDR, Reynolds number, metabarcoding, ZooScan

ABSTRACT

Swimming and sinking behavior by pelagic snails is poorly studied but is important in their ecology, predator-prey interactions, and vertical distributions. We used a low magnification, high speed stereophotogrammetry system to study the swimming and sinking kinematics of nine warm water pelagic snail species (seven thecosomes, one gymnosome, and one heteropod). As different thecosomatous pteropod species may have coiled, elongated, or globular shell morphologies, we focused on how the shell shape, body geometry, and body size affect their swimming behavior from a fluid mechanics perspective. In addition, ZooScan image analysis and metabarcoding of archived vertically stratified MOCNESS samples were used to relate swimming behaviors to night time and daytime vertical distributions. While different large scale swimming patterns were observed, all species exhibited small scale sawtooth swimming trajectories caused by reciprocal appendage flapping. Thecosome swimming and sinking behavior corresponded strongly with shell morphology and size, with the tiny coiled shell pteropods swimming and sinking the slowest, the large globular shelled pteropods swimming and sinking the fastest, and the medium-sized elongated shell pteropods swimming and sinking at intermediate speeds. However, the coiled shell species had the highest normalized swimming and sinking speeds, reaching swimming speeds of up to 45 body lengths s^{-1}. The sinking trajectories of the coiled and elongated shell pteropods were nearly vertical, but globular shell pteropods use their hydrofoil-like shell to glide downwards at approximately 20° from the vertical, thus retarding their sinking rate. The swimming Reynolds number (*Re*) increased from the coiled shell species ($Re \sim O(10)$) to the elongated shell species ($Re \sim O(100)$) and again for the globular shell species ($Re \sim O(1000)$), suggesting that more recent lineages increased in size and altered shell morphology to access greater lift-to-drag ratios available at higher *Re*. Swimming speed does not correlate with the vertical extent of migration, emphasizing that other factors, likely including light, temperature, and predator and prey fields, influence this ecologically important trait. Size does play a role in structuring the vertical habitat, with larger individuals tending to live deeper in the water column, while within a species, larger individuals have deeper migrations.

Includes: 10,025 words, 11 figures and 3 tables.

INTRODUCTION

Pteropods and heteropods are small (mm to cm scale) marine snails that may be found in mesopelagic to surface waters throughout the global ocean. Of the extant holoplanktonic molluscs, heteropods and pteropods are the most numerous and diverse, playing a role in food web structure and in carbon and carbonate export (Gilmer, 1972; Lalli and Gilmer, 1989; Hunt et al., 2008). Thecosomatous pteropods in particular maintain a large biomass in some regions and appear to have a substantial biogeochemical role in carbonate and carbon cycling (Bednaršek et al., 2012; Buitenhuis et al., 2019). Gymnosomes pteropods and heteropods are substantially less abundant but are ecologically important as they are active predators of other zooplankton, including the thecosomes.

Pteropods consist of two orders that include both the thecosomatous species, which are generally shelled as adults, and the gymnosomatous species, which lose their juvenile shell during development (Lalli and Gilmer, 1989; Peijnenburg et al., 2019). The shells of thecosomes vary dramatically by species, ranging from the basal spiral form, to conical, globular, and gelatinous forms. Two of the three families of heteropods have shells as adults, and although they are consistently spiral in shape, they are distinctly different in size and function. In the most numerous family, the Atlantidae, the adult individuals can retract completely into the dorsoventrally flattened shell, while in the larger more streamlined Carinariidae the dorsally oriented shell is substantially smaller than the body. Despite being from two distinct molluscan lineages, all three groups build shells composed of aragonite during some portion of their development, and use highly flexible appendages that are derived from the basal molluscan foot structure for locomotion (Lalli and Gilmer, 1989). In the pteropods the foot has evolved into a pair of muscular, wing-like appendages, while heteropods have a single muscular swimming appendage which, in Atlantidae, coordinates with the shell for swimming (Karakas et al., 2018).

These zooplanktonic marine snails are famously difficult to study, and most species currently cannot be cultured (Howes et al., 2014; Thabet et al., 2015). Thus, detailed study of much of their biology, ecology, and behavior has been limited. For instance, in most groups swimming, a key behavior for pelagic organisms, has not been assessed. In the zooplankton, swimming influences predator-prey dynamics, both moderating escape and hunting behavior, but also controlling the process of diel vertical migration. This migratory phenomenon is a common feature in pelagic ecosystems, whereby organisms actively congregate in the surface waters during the night to feed, and then descend to depth during the day. These daily migrations are thought to be energetically expensive, with pteropods and heteropods smaller than 1 cm traveling hundreds of meters per day (Wormuth, 1981; Maas et al., 2012; Wall-Palmer et al., 2018). Despite the costs, the process is believed to provide a number of advantages including niche partitioning, metabolic advantage due to colder temperatures at depth, avoidance of light or high temperatures, and, most importantly, predator avoidance (Hays, 2003; Antezana, 2009).

Even though it is challenging to study the pelagic marine snails, some previous research has been carried out on marine snail swimming, mostly on polar species with limited morphological or taxonomic diversity. In the gymnosomes, Satterlie et al. (1985) investigated *Clione limacina* swimming and noticed that this gymnosome flaps its wings back and forth in the dorsoventral plane with a high angle of attack and suggested that *C. limacina* may generate lift using the ‘clap-and-fling’ mechanism described by Weis-Fogh (1973) in flying insects. Childress and Dudley (2004) investigated the critical flapping Reynolds number that

enables *Clione antarctica* to propel itself by wing flapping. Borrell et al. (2005) studied the swimming kinematics of *Clione antarctica* and observed a sawtooth path during upward swimming. Szymik and Satterlie (2011) conducted experiments on *C. limacina* at slow and fast swimming speeds, and found that the wingbeat kinematics differ significantly between speeds. In the thecosomes, Chang and Yen (2012) found that *Limacina helicina* ascends along a sawtooth trajectory in mostly linear and sometimes helical swimming paths, but has straight sinking trajectories. *L. helicina* strokes its wings in a characteristic figure-of-eight pattern by extreme rotation of its body to produce lift (Murphy et al., 2016). Similar swimming characteristics such as sawtooth swimming trajectories and extreme body rotation were also observed in the closely related polar species *Limacina helicina antarctica* (Adhikari et al., 2016), and Mohaghar et al. (2019) performed a dimensional analysis of the swimming of this species. Morton (1954) described the swimming behavior of *Limacina retroversa* qualitatively, and more recently Bergan et al. (2017) conducted quantitative measurements of the swimming and sinking kinematics of the same species under the influence of elevated carbon dioxide, which alters shell properties. Karakas et al. (2020) showed that the tropical thecosome *Cuvierina atlantica* uses its highly flexible parapodia in a cylindrical overlap-and-fling mechanism twice during each stroke to generate lift. In the heteropods, Karakas et al. (2018) discovered that, contrary to previous accounts (Lalli and Gilmer, 1989), the atlantiid heteropod *Atlanta selvagensis* does not let its shell passively hang beneath it as it swims but instead flaps its shell in coordination with its swimming fin in order to swim. Finally, Zhou and Mittal (Zhou and Mittal, 2017, 2018) used computational fluid dynamics simulations to examine the swimming behavior of the distantly related shell-less marine mollusks *Hexabranchus sanguineus* (the Spanish Dancer) and *Aplysia* (the sea hare), which are much larger than the pteropods and heteropods studied here.

Recent studies suggest that ocean acidification-induced changes to shell thickness or morphology may change pteropod swimming behavior, thus negatively affecting their ability to perform diel vertical migration. For example, Manno et al. (2012) claimed that a lower pH environment in combination with lower salinity negatively affected upward swimming ability of the pteropod *Limacina retroversa*. Ocean acidification may damage the pteropod shell, thus unbalancing the forces and torques involved in the animal swimming and thereby altering the swimming kinematics and fluid dynamics of swimming (Adhikari et al., 2016).

It has been posited that sinking may also be an important behavior for these pelagic marine snails in relation to their daily migration or predator avoidance. The aragonite shells of these animals make them extremely negatively buoyant, and for many species of shelled thecosomes or atlantid heteropods, disturbance causes retraction into the shell and rapid sinking behaviors (Gilmer and Harbison, 1986; Bergan et al., 2017). This negative buoyancy additionally strongly influences their role as important contributors to the active flux of carbon and carbonate from surface waters, as it increases the rate at which dead organisms are removed from the mixed layer and sequestered at depth. Importantly, the rapid sinking may allow shells to penetrate below the aragonite lysocline prior to dissolving, augmenting their export efficiency. Additionally, sinking can be energetically problematic as organisms must counteract their negative buoyancy to avoid sinking away from their desired vertical habitat.

Although thecosomes have been observed making large mucous webs that help them slow their sinking (Harbison and Gilmer, 1992), heteropods do not have this adaptation. However, Bergan et al. (2017) observed reduction in sinking speed when *L. retroversa* was filmed

sinking with its wings extended compared to when a live animal sank with wings retracted. This suggests that pelagic snails can use their appendages to reduce their sinking speed.

Characterizing the behaviors associated with sinking and swimming in these groups thus has both ecological and biogeochemical significance. To date, however, most previous research has focused on high latitude species (e.g. *Limacina helicina*, *Limacina helicina antarctica*, *Limacina retroversa*, *Clione limacina*, and *Clione antarctica*). In polar regions, pteropods in particular are highly abundant, but there is little speciation and thus little variety in shell shape. In contrast, warm water regions are highly diverse, supporting a large variety or marine snails with distinct shell shapes and sizes (Burridge et al., 2017). Here we investigate the swimming and sinking kinematics of a large number of warm water thecosome species. We additionally investigate the swimming kinematics of a co-occurring gymnosome species and one atlantid heteropod species. The objective is to provide basic kinematic parameters across a range of species and to investigate the biomechanics of how swimming and sinking characteristics vary with shell shape and size. We then use imaging and metabarcoding techniques to detail the vertical habitat and migratory patterns of the pteropod species to explore how morphology and swimming biomechanics are related to distribution.

MATERIALS AND METHODS

Marine snails were collected offshore of Bermuda from a small boat using a Reeve net with 150 μm mesh size and a specialized 20 L cod end. Specimens were collected during nighttime cruises in May and September of 2017 and in May 2019. Animals were kept in the collected seawater for less than 1 hour during the transit back to shore where they were quickly and gently isolated from the cod end. Individuals were visually checked for damage and species identification under a stereomicroscope, then stored in 1 L jars containing filtered seawater at an *in situ* temperature of 21 ºC and salinity of 36 psu. Data collection began immediately upon return from the cruise, and most experiments were completed within one day of collection.

A photogrammetry system comprising two synchronized high-speed monochrome Edgertronic cameras (Sanstreak Corp., San Jose, CA, USA) was used to measure the three-dimensional swimming trajectories of the organisms at low magnification (Figure *1*)Figure *2*. The cameras, lights, and aquarium were mounted on optical rails and a breadboard to rigidly support the system. Two 50 mm Nikon lenses at f/32 aperture and fiber optic illuminators with Fresnel lenses (focal length of 76.2 mm, part #32-593, Edmund Optics) were used to provide the field of view. A variety of pteropod and heteropod species were placed in an aquarium with 152.4×152.4×152.4 mm^3 inner dimensions and 6.35 mm wall thickness. This low magnification system provides a field of view at least ten times larger than the largest animal of interest, thus allowing measurement of 15 to 20 full stroke cycles of upward swimming. The spatial resolution of the cameras was 98.4 μm $pixel^{-1}$ and the temporal resolution was 1.67 ms (corresponding to 600 frames per second). In a few videos, a frame rate of 300 frames per second was used. The low magnification stereophotogrammetric system was calibrated using the sparse bundle adjustment (SBA) method (Lourakis and Argyros, 2009) as implemented in Argus 3D (Jackson et al., 2016), in which a calibration wand was moved throughout the tank volume. The camera system was manually triggered when an animal swam into the field of view common to both cameras.

Ninety five videos of swimming marine snails ranging in length from 2 to 14 s were recorded. Videos were recorded of seven thecosome species (*Heliconoides inflatus*, *Limacina*

bulimoides, *Cuvierina atlantica, Hyalocylis striata, Diacria trispinosa, Styliola subula, Creseis clava*), one gymnosome species *Pneumoderma atlantica*, and one unidentified atlantiid heteropod. Thecosome species which were captured but which could not be recorded swimming included *Diacria quadridentata*, *Diacavolinia longirostris, Limacina leuserii* and *Creseis conica.* Recorded videos were divided into segments in which the animal was either sinking or swimming. Sinking was defined as when the animal completely ceased wing motion, resulting in downward motion. A video segment in which any wing motion was observed was classified as swimming, regardless of the resulting swimming direction. Table 1 shows the number of swimming and sinking segments recorded for each species. Since many animals were added to the aquarium at once, it was not always possible to determine the individual identity of each animal. Table 1 thus gives the estimated minimum number of individual animals of each species based on factors such as experiment date, animal length, and multiple animals of the same species simultaneously in the camera view. In order to measure swimming trajectories, one point in the center of the animal body was digitized in DLTdv software (versions 5,7, and 8; Hedrick 2008). Three dimensional swimming and sinking trajectories of the animal are thus reconstructed from the 2D camera coordinates. A global (XYZ) coordinate system is defined for trajectory analysis in which the XY plane is horizontal and the positive Z component is directed upward. Figure 2 shows CAD models representing each of the recorded species and the measured body length L. In two species (e.g. *H. inflatus*, *L. bulimoides*), L represents the shell length, which corresponds to the longest dimension of the animal. In the other thecosome species, L includes the shell and the proximal portions of the parapodia. The length L was measured by digitizing the two corresponding points on the animal over at least 20 consecutive frames in DLTdv5 software (Hedrick, 2008). The wingspan L_f (measured from wingtip to wingtip at the time point when the wings were fully extended) was similarly measured for *D. trispinosa*, *S. subula*, *C. clava*, *Pneumoderma atlantica*, and the heteropod species. Values of L_f for the other four species were similarly obtained from videos from the high magnification photogrammetry system described in Karakas et al. (2018).

Instantaneous swimming or sinking speed was calculated using the forward difference technique across consecutive time points. Mean swimming speed U and sinking speed U_{sink} for each trajectory were calculated by averaging the animal's speed over the entire extent of that trajectory. Species-specific swimming and sinking speeds $\overline{U}$ and $\overline{U}_{sink}$ were calculated by averaging the mean values of U and U_{sink} across all recorded trajectories for each species. Normalized swimming speeds U' and sinking speeds U'_{sink} were calculated for each trajectory by dividing the U or U_{sink} by the corresponding animal's length L. Species-specific normalized swimming and sinking speeds $\overline{U}'$ and $\overline{U}'_{sink}$ were calculated by averaging the mean values of U' and U'_{sink} across all recorded trajectories of each species in the same life stage. The vertical component of sinking speeds $\overline{U}_{sink}$ and $\overline{U}'_{sink}$ also were calculated. A mean body length $\bar{L}$ was calculated for each species by averaging L across all recorded trajectories. Mean beat frequency f for each trajectory was determined in ImageJ as the average beat frequency over at least 10 full wingbeat cycles. Videos from the high magnification photogrammetry system described in Karakas et al. (2018) also were used to acquire additional data on wingspan, and wingbeat frequency. In addition, the net-to-gross displacement ratio (NGDR), a measure of trajectory tortuosity, was determined for swimming behaviors. NGDR is defined as the ratio of the distance between the starting and ending points of the trajectory divided by the total distance traveled between the starting and ending points. Because this metric is scale dependent, NGDR was calculated over a distance of five body lengths for each species. Thus, NGDR was calculated for five body length along each trajectory starting from the beginning of that trajectory. NGDR values could not be calculated

for all recorded trajectories because some trajectories were less than five body lengths. Because many of the animals experienced some horizontal displacement as they sank, a glide angle α was also measured for the sinking trajectories, where α is the acute angle between the vertical axis and a line representing the total displacement. Finally, the body-based Reynolds number Re=UL/ν of each swimming animal was calculated, where the kinematic viscosity ν of seawater at 21º C is taken as 1.02×10^{-6} m^2 s^{-1}. A sinking Reynolds number $Re_{sink}=U_{sink}L/\nu$ also was calculated.

One-way analysis of variance (ANOVA) was used to examine differences in the mean swimming speed, mean sinking speed, mean normalized swimming speed, mean normalized sinking speed, glide angle, and NGDR among the different thecosome shell groups (e.g. coiled, elongated, and globular), with a significance testing value of 0.05. Further, the Tukey-Kramer pair wise comparison test was used for multiple comparisons of these parameters among these groups. All statistical calculations and evaluations of data were performed in MATLAB (v9.6 R2019a, The MathWorks Inc., MA).

To provide ecological context for our measurements we analyzed the vertical distribution of pteropods and heteropods using archived 1 m Multiple Opening/Closing Net and Environmental Sensing System (Wiebe et al., 1985) samples. These samples were collected with 150 µm nets that were deployed during the mid-day and mid-evening on cruises carried out in July of 2016, 2017, 2018, and 2019 as well as October 2018, from 0-1000 m in the vicinity of the Bermuda Atlantic Time Series (sampling details provided in Supplementary File 1). This resulted in six night time profiles and eight daytime profiles of the water column. Upon retrieval, the catch from each of the eight discrete nets was divided into splits and half was preserved in buffered 4% formalin in seawater. A subset of this sample was imaged and measured, and marine snails were taxonomically classified using a ZooSCAN ver. 3 at 4,800 dpi and the ZooProcess pipeline (Gorsky et al., 2010; Vandromme et al., 2012). All images representing pelagic snails were identified to species and only those that clearly had a body in the shell (more likely to represent a live individual) were enumerated. These were converted to abundances by applying the volume filtered and split counts to generate daytime and night time vertical distributions of adult individuals. The distribution was plotted as abundance per size bin (using major axis in mm) using the “violin plot” option of the ggplot2 packing in R.

Although the ZooSCAN method provides numerical counts and size class distributions for individuals, it is constrained by the fact that pteropods are relatively rare members of the zooplankton community. Additionally, it can be difficult to assign a species to some images, particularly for the smaller size classes. To augment our distributional analyses we additionally employed metabarcoding techniques on one MOCNESS tow pair. This tool provides species-specific identification and is more likely to sample rare individuals in the tows. Ethanol-preserved samples from July 2017 were analyzed following a metabarcoding protocol similar to Blanco-Bercial (2020) but interrogating the V1-V2 region of the 18S rDNA gene, using the primers described in Fonseca et al. (2010). Briefly, half of the ethanol sample was ground with a homogenizer, treated with proteinase K, and DNA was extracted using a SDS-chloroform protocol (OMEGA EZNA DNA Mollusk kit). Three PCR reactions were done for each sample with custom adapters and the resulting products were pooled by sample and sent to University of Rochester for sequencing using the MiSeq Reagent Kit v2 (500-cycles; 2 x 300) V2 chemistry.

Sequence data was processed as in Blanco-Bercial (2020), with initial cleaning and alignment with MOTHUR (Schloss et al., 2009). Relative counts for all samples were standardized to 20,000 reads sample^{-1} and values below 1 discarded. Taxonomic units were built at 100% similarity after accounting for PCR error using Deblur (Amir et al., 2017) and a SILVA-derived custom 18S database was used to feed MOTHUR for the OTU assignment using the nr database from SILVA (see Blanco-Bercial, 2020). Pteropod taxonomy was confirmed by BLAST (March 22, 2020) and by phylogenetic placement using RAxML ver. 8 and mrBayes (Ronquist et al., 2012; Stamatakis, 2014) as in (Maas et al., 2013), using an alignment created with sequences available from GenBank for "Pteropoda 18S" and adding some other Euopisthobranchia as outgroups. The sequence relative abundances were weighed against the measured total live biovolume (calculated from paired image dataset; see above), then calculated per square meter. This results in the proportional contribution of a particular sequence per mm^3 of living biovolume throughout the water column. The distribution of OTUs present in more than four samples were analyzed and plotted to assess diel vertical migratory patterns.

RESULTS

Figure 3 and Figure *4* show representative 3D upward swimming trajectories and Figure 5 shows representative 3D sinking trajectories of the marine snails (i.e. 7 thecosomatous pteropods, 1 gymnosomatous pteropod, and 1 atlantiid heteropod) investigated in this study. These trajectories, along with data on shell length, swimming speed, wingbeat frequency, and *Re* presented in Table 2, will be used to describe the swimming kinematics of each species.

The thecosome *Heliconoides inflatus* (Figure 2a) has a flattened coiled shell with a thickened rib on the outer margin, and a body length of 0.9-1.2 mm and flaps it parapodia at 6.6-11.1 Hz, resulting in swimming speeds of 12-51 mm s^{-1} and *Re*=12-66 (Table 2). As seen in Figure 3, small-scale trajectory oscillations are particularly evident in this species. These oscillations are due to individual power and recovery strokes by the swimming appendages which cause extreme pitching of the shell, resulting in a sawtooth swimming trajectory in which the animal may even sink at the end of each half stroke (Adhikari et al., 2016; Murphy et al., 2016; Karakas et al., 2018). At the large scale, *H. inflatus* exhibits a characteristic upwards helical swimming trajectory and also often exhibits a circular swimming trajectory in the horizontal plane, features that are often seen in other swimming zooplankton such as copepods (Bianco et al., 2014). However, this species may also swim in a straight line, thus showing some behavioral variety in its swimming. Figure 5 shows that *H. inflatus* has a fairly straight downward sinking trajectory, sinking at speeds of 13-22 mm s^{-1} and corresponding sinking Reynolds number of Re_{sink}=12-29 (Table 2). While sinking, the wings of *H. inflatus* remain extended upwards, thus keeping this species largely in an upright posture.

The thecosome *Limacina bulimoides* (Figure 2b) has a high spiraled shell and a body length of 1.3-1.4 mm and flaps it parapodia at 8.8-12.9 Hz, resulting in swimming speeds of 18-40 mm s^{-1} and *Re*=22-51 (Table 2). This species is similar in size and swimming speed to *H. inflatus* and, as seen in Figure 3, exhibits similar small-scale trajectory oscillations. However, at the large scale, *L. bulimoides* does not seem to exhibit the helical swimming patterns seen in *H. inflatus*. Figure 5 shows that *H. inflatus* also has a straight sinking trajectory, sinking at speeds of 16-19 mm s^{-1} and corresponding sinking Reynolds number of Re_{sink}=22-25 (Table 2). While sinking, the wings of *L. bulimoides* also remain extended upwards, but the shell is oriented horizontally.

The thecosome *Cuvierina atlantica* (Figure 2c) has an urn- or bottle-shaped shell and a body length of 8.5-10.6 mm and flaps it parapodia at 4.7-6.2 Hz, resulting in swimming speeds of 13-46 mm s^{-1} and *Re*=124-434 (Table 2). As such, *C. atlantica* is much larger than the two previously described thecosomes but swims at a similar speed, thus operating in a Reynolds number regime that is an order of magnitude higher. In addition, *C. atlantica* flaps it parapodia at a slower rate than the two smaller thecosomes. Similar to the two previously described thecosomes, *C. atlantica* exhibits small-scale oscillations in its trajectory owing to individual power and recovery strokes. In addition, *Cuvierina atlantica* swims in a characteristic upright posture with its seemingly heavy shell hanging downwards and oscillating like a pendulum. At the large scale, *C. atlantica* also often exhibits a spiral upwards swimming trajectory (not shown). This species may also swim sideways, but when doing so, its elongated shell always hangs beneath it. *Cuvierina atlantica* rapidly sinks downwards when it stops flapping, at speeds of 19-53 mm s^{-1} and corresponding sinking Reynolds number of Re_{sink}=305-535 (Table 2). While sinking, the shell of *C. atlantica* usually reorients from a vertical to a horizontal orientation (with wings still extended), often resulting in a significant glide angle. In some cases, the downward sinking trajectory of *C. atlantica* forms a tight spiral (e.g. Figure 5).

The thecosome *Hyalocylis striata* (Figure 2d) has a very thin ribbed conical shell and a body length of 6.8-6.9 mm and flaps it parapodia at 7.6-8.1 Hz, resulting in swimming speeds of 18-28 mm s^{-1} and *Re*=116-191 (Table 2). With its relatively large shell and high swimming speed, *H. striata* swims at a Reynolds number comparable to that of *C. atlantica*. The thecosome *H. striata* gives the impression of being a much stronger swimmer than the previously described thecosomes. For example, *H. striata*, though of comparable size, is much more maneuverable and agile than *C. atlantica* and does not seem to have a characteristic body position when swimming. Rather, it is capable of easily swimming in any direction and was often observed actively swimming downwards. Further, the small-scale oscillations seen in the previously described thecosomes are almost absent in *H. striata*, leading to a much smoother swimming trajectory (Figure 3). The sinking speed of *H. striata* is in the range of 24-26 mm s^{-1} with a corresponding sinking Reynolds number of Re_{sink}=158-183, and this species largely exhibits a straight downwards sinking trajectory. While sinking, the shell of *H. striata* remains in a vertical position with no shell reorientation. The wings are initially held outwards but later turn upwards, acting to streamline the organism.

The thecosome *Diacria trispinosa* (Figure 2e) has a globular but dorsoventrally flattened shell with one posterior and two lateral spines. Further, *D. trispinosa* has a body length of 11.6-13.9 mm and flaps it parapodia at 4.9-6.8 Hz, resulting in swimming speeds of 58-114 mm s^{-1} and *Re*=680-1567 (Table 2). With the largest body size and highest swimming speed of the marine snails tested, *D. trispinosa* also swims at the highest Reynolds number. *Diacria trispinosa* gives the impression of being a much stronger swimmer than the other thecosomes and may easily swim in any direction. This species characteristically swims upwards in a straight line at an average climbing angle of 47.5±8.7° (mean ± standard deviation; n=5) to the horizontal plane (Figure 4). The sinking behavior of *D. trispinosa* is unique among the thecosomes. With its wings bending upwards, this species reorients from a vertical to a horizontal shell orientation when sinking, resulting in a trajectory that significantly deviates from the vertical. Thus, *D. trispinosa* sinks with a glide angle of 21.7±10.1° (mean ± standard deviation; n=3) from the vertical. This behavior seems to be enabled by the flattened shell of *D. trispinosa*, which acts as a hydrofoil to generate lift during the descent. The sinking speed of *D. trispinosa* is thus in the range of 60-105 mm s^{-1}, with a corresponding sinking Reynolds

number of Re_{sink}=830-1150 (Table 2), but would likely be higher in the absence of this gliding behavior.

The thecosome *Styliola subula* (Figure 2f) has a conical shell, with a thickened longitudinal spine running along the dorsal length. Further, *S. subula* has a body length of 3.6-8.7 mm and flaps it parapodia at 6.1-10.5 Hz, resulting in swimming speeds of 17-63 mm s^{-1} and *Re*=60-505 (Table 2). The sinking speed of *S. subula* is 22-52 mm s^{-1} with a corresponding sinking Reynolds number of Re_{sink}=348-417 (Table 2). The sinking behavior of *S. subula* was similar to that of *H. striata*, with a vertical orientation and the wings extended upwards. The large range of sizes and other parameters for this species reflects the fact that videos of a juvenile and an adult were captured. In general, the morphology and swimming style of *S. subula* are very similar to that of *H. striata* with the exception that the shell of *S. subula* seems bulkier and possibly heavier than that of *H. striata*. This difference is reflected in the larger sinking speed of *S. subula* and in the fact that *S. subula* seems less agile and maneuverable than *H. striata*.

The thecosome *Creseis clava* (Figure 2g) has an extremely elongated, needle-like shell and an extremely short wingspan relative to its body length. Further, *C. clava* has a body length of 6.8-7.2 mm and flaps it parapodia at 10.5-13.8 Hz, resulting in swimming speeds of 33-40 mm s^{-1} and *Re*=238-278 (Table 2). It is worth noting that *C. clava* has the highest wingbeat frequency of all the studied thecosomes. With its elongated shell, *C. clava* has an upright swimming posture similar to that of *C. atlantica* and is not maneuverable. Further, *C. clava* exhibits high frequency small-scale oscillations in its trajectory similar to those of *C. atlantica* (Figure 4). No videos of *C. clava* sinking behavior were acquired.

The gymnosome *Pneumoderma atlantica* (Figure 2h) has an elongated soft body without the protection of a shell. *Pneumoderma atlantica* has a body length of 11.5-13.1 mm and flaps its wings at 3.5-4.5 Hz, resulting in swimming speed of 11-34 mm s^{-1} and *Re*=134-438 (Table 2). Similar to many of the thecosome species, this gymnosome exhibited small-scale oscillations in its trajectory as a result of individual wing strokes. This agile species was often observed swimming upwards in a spiral but was also observed to hover in an upright posture at the same elevation for long periods of time and to actively swim downwards. No videos of sinking behavior were acquired for this species, but, due to its lack of shell, its sinking speed would presumably be much less than that of the shelled pteropods.

The heteropod species (Figure 2i) has a single swimming fin above the body and a downward hanging shell which functions as a second appendage that flaps synchronously with the fin to propel the animal (Karakas et al., 2018). The heteropod has a body length of 2.3-3.3 mm and flaps its parapodia at 9.3-9.6 Hz, resulting in swimming speeds of 22-35 mm s^{-1} and *Re*=52-117 (Table 2). Small-scale side-to-side oscillations are observed in this animal's trajectory owing to individual strokes of its fin and shell. Though this heteropod species is negatively buoyant, no sinking behavior was observed in the current study.

Figure 6a and Figure *6*b show the mean and standard deviation of the swimming speeds U and U', respectively, as a function of body length L for each recorded trajectory for all the marine snail species. Figure 6c and Figure *6*d show swimming speeds $\overline{U}$ and $\overline{U}'$ for each species as a function of $\overline{L}$. Figure 6a shows that L is tightly grouped into three classes corresponding to thecosome shell morphology. Coiled shell thecosomes (*H. inflatus* and *L. bulimoides*) have shell sizes ranging from 0.9 to 1.4 mm. Elongated shell thecosomes (*H. striata*, *C. atlantica*, *C. clava*, and *S. subula*) have shell sizes ranging from 6.8 to 10.6 mm

(with the exception of a juvenile *S. subula* excluded from the calculation of $\bar{L}$). The single globular shell species (*D. trispinosa*) has shell sizes ranging from 11.6 to 14.0 mm. The mean of each of these groups also is shown in Figure 6c and Figure 6d. Swimming speeds of individual species within these three classes do not differ much from each other. For example, no significant difference was found among the four species comprising the elongated shell group (P >0.05, one-way ANOVA). However, swimming speed across the groups differs significantly as shown in Figure S1A (F=75.62, P < 0.001). The coiled shell, elongated shell, and globular shell pteropods have mean swimming speeds of 27.2, 33.5, and 83.7 mm s^{-1}, respectively, thus showing an increase with body length. A follow up Tukey-Kramer pairwise comparison test shows that all three shell groups are significantly different from the others (Table S1). However, the normalized swimming speeds of the coiled shell pteropods are greatest, with $\overline{U}'$=22.7 BL s^{-1} and a maximum U' of 45 BL s^{-1} for one individual of *H. inflatus*. In contrast, the normalized swimming speeds of the elongated shell pteropods are the least (4.3 BL s^{-1}), and the normalized swimming speeds of the globular shell pteropods are in between (6.6 BL s^{-1}). The coiled shell group has a significantly larger normalized mean swimming speed as confirmed by the one-way ANOVA (F=123.25, P < 0.001, Figure S1B), and the paired Tukey-Kramer test shows a significant difference between the coiled and elongated shell groups and between the coiled and globular shell groups (P<0.001), but there is no statistically significant difference between the elongated and globular shell groups (P=0.495, Table S1). The heteropod has a coiled shell which is similar in size that of the coiled shell thecosomes and a mean swimming speed of 28.7 mm s^{-1}. However, owing to its completely different swimming style, the heteropod does not group with the coiled shell thecosomes in Figure 6. In addition, the gymnosome, though shell-less and of similar size to *D. trispinosa*, swims much slower (18.1 mm s^{-1}). As expected, swimming speed generally increases with increasing beat frequency for all species, as shown in Figure S2 (though this trend is not seen for *D. trispinosa*).

Figure 7a and Figure 7b show the mean and standard deviation of the sinking speeds U_{sink} and U', respectively, as a function of body length L for each recorded trajectory for all the marine snail species. Figure 7c and Figure 7d show sinking speeds $\overline{U}$ and $\overline{U}'$ for each species as a function of $\bar{L}$. In each panel, the hollow symbols represent the sinking speed and the filled symbols represent the vertical component of sinking speed. As seen in Figure 7a, sinking speeds generally fall into three classes corresponding to coiled, elongated, and globular shell morphologies. However, in contrast to swimming speed, sinking speed clearly increases with body size. Mean sinking speed across the groups differs significantly as shown in Figure S1C (F=129.56, P < 0.001) as the globular shell pteropod has a higher sinking speed (86.2 mm s^{-1}) than the elongated (40.9 mm s^{-1}) and coiled (17.1 mm s^{-1}) shell groups. Similar to the mean swimming speed, the mean sinking speed between each pair is also significantly different from each other (P<0.001 for each pair, Table S1). For both the coiled and elongated shell pteropods, minimal differences are seen between the sinking speed and the vertical component of the sinking speed (vertical components are 96% and 87% of the sinking speed, respectively). These minor differences are possibly due to drag and lift forces on the shells and outstretched wings as the animals sink. These unbalanced forces may cause, for example, the helical sinking trajectories observed for *C. atlantica*. In contrast, the globular species *D. trispinosa* has a much larger difference between its sinking speed and the vertical component of its sinking speed (83%) due to the gliding behavior described earlier. A similar pattern for normalized swimming speed among the three groups is also seen for the normalized sinking speed. The coiled shell species have the largest normalized sinking speed (13.7 BL s^{-1}) whereas the elongated shell group has the smallest (4.1 BL s^{-1}), and the globular shell species

falls between (6.0 BL s^{-1}). Similar to the normalized mean swimming speed, there are also significant difference in the normalized mean sinking speed between different groups ($F=105.79$, $P < 0.001$, Figure S1D). Again, the normalized mean sinking speeds of the coiled shell and elongated shell pair and the coiled shell and globular shell pair are significantly different ($P<0.001$ for both pairs), whereas that of the elongated shell and globular shell pair are not significantly different ($P=0.393$, Table S1).

Figure 8a shows the glide angle α measured from each recording as a function of L. Figure 8b shows the mean glide angle for each species and each shell morphology as a function of $\bar{L}$. The coiled shell species *H. inflatus* and *L. bulimoides* have $\alpha<10°$, reflecting the fact that they sink almost vertically. As a group, the coiled shell pteropods have a mean glide angle of 4.1° (Figure S3A). Values of α for the elongated species are slightly greater, with most falling in the range of $1°<\alpha<15°$ and a few outliers with values up to almost 30° (Figure S3A). The mean glide angle for the elongated shell pteropods is 7.7°. The globular shell species *D. trispinosa* sinks at glide angles up to 31.6° and has a mean glide angle value of 21.7° (Figure S3A). This large glide angle is due to lift generated by the unique shell shape of *D. trispinosa* and by its partially outstretched wings. The one-way ANOVA test shows that a significant difference exists in the glide angles of the coiled, elongated, and globular shell groups ($F=14.57$, $P < 0.001$, Figure S3A). Further, the Tukey-Kramer pairwise tests showed significant differences between each pair (Table S1).

Figure 9 shows mean values of NGDR over a distance of five body lengths for each species as a function of $\bar{L}$. Values of NGDR for all thecosome species except for *D. trispinosa* are fairly similar and fall within the range of 0.6 to 0.7. The one-way ANOVA test showed a significant difference among the three shell groups for the mean NGDR values ($F=6.23$, $P = 0.003$, Figure S3B). A follow up pairwise comparison showed there is no significant difference between the coiled shell and elongated shell groups ($P=0.636$, Table S1) but that there is a significant difference between the globular shell group and the other two groups. These relatively low values for the coiled and elongated shell species represent the tortuous 'sawtooth' trajectories induced by individual power and recovery strokes. In contrast, *D. trispinosa* has a much higher NGDR of 0.89. This species is a much stronger swimmer, operating at an order of magnitude higher Reynolds number (Table 2), and its dorsoventrally flattened shell may help damp out the small-scale pitching oscillations observed in smaller pteropods. The heteropod had an elevated NGDR value of 0.81, whereas *P. atlantica* had a NGDR value (0.65) that was more similar to the thecosomes. Because NGDR was calculated over only five body lengths, these values represent the small-scale oscillations in their swimming trajectories and not large-scale swimming patterns. Values of NGDR at larger spatial scales would be useful but could not be calculated here because recorded swimming trajectories varied in length. Using all recorded trajectories regardless of length would have introduced a bias since NGDR is a scale-dependent parameter (Seuront et al., 2004). Bergan et al. (2017) calculated tortuosity, which is the inverse of NGDR, for the coiled shell species *Limacina retroversa* which is morphologically similar to *L. bulimoides* and *H. inflatus*. These authors found corresponding mean NGDR values of 0.49 to 0.79. While these values are similar to those of the coiled shell pteropods, it is difficult to make a direct comparison because these authors do not report the trajectory lengths over which NGDR was calculated.

Only four of the species we filmed were sufficiently abundant in the MOCNESS samples to allow for statistically meaningful assessment of their size-based distributions (Figure 10). Of the remainder of the groups they could either not be identified to species via the images (gymnosomes and atlantid heteropods), or were sampled too infrequently to reliably

determine size-based day and night distributions. For some species there was a clear difference in depth habitat based on size with longer individuals found at deeper depths, including *H. inflatus*, *C. clava*, and *S subula.*

Metabarcoding analyses confirmed the species identification made by the ZooSCAN and additionally allowed for better discrimination between taxa that are morphologically similar, providing a better context for the vertical distribution of the various species. Despite the fact that metabarcoding analyses were conducted on only one of the day and night pairs of MOCNESS tows that were analyzed for images, the patterns in distribution were similar overall and were consistent with findings in the previous literature (Table 3; Supplementary Figure S4). Discrepancies between molecular methods and previous findings appear to be more common in the larger species that are rare and therefore more poorly sampled. The use of paired image and barcoding allowed for greater understanding of the dataset, suggesting, for example, two gymnosome species with non-overlapping vertical distributions. The first, identified as *Pneumoderma atlantica*, was likely the species captured and used for our video analysis. Adults of this group appear to migrate from a daytime depth of 50-200 m to a night time habitat of 0-200 m. The other, an unidentified gymnosome, has a midwater habitat from 300-700 m. An uncertain problem is that metabarcoding did not detect *Limacina bulimoides*, despite its documented presence in the samples. The most plausible explanation would be a highly divergent sequence for this species, which might have affected its amplification efficiency during the PCR protocols due to mutations in the primer regions.

Of the species filmed in this study, there were a range of migratory patterns. The species with the widest vertical distribution (found abundantly from 50-400 m, but as deep as 550-700 m) was *D. trispinosa*. Similarly, *C. atlantica* (barcoded as *C. columnella*) was found from 0-400 m, although it was found most abundantly at 300-400 m. These two larger species were rarely captured in images, and both were under sampled at night (particularly in the metabarcoding analysis) making definitive characterization of diel migration patterns difficult. Our data suggests that all species used in this study are migratory, traveling 50 to 300 m per day. The extent of migration was not correlated with average species length, the swimming speed, or sinking speed.

DISCUSSION

Planktonic marine snails in warm waters have diverse shell and body geometries and sizes which affect their swimming abilities and sinking characteristics. Indeed, within a shell group (i.e. coiled, elongated, or globular), the various thecosome species studied here had similar sinking and swimming characteristics. Coiled shell species are the smallest thecosomes and swim and sink the slowest but have the highest normalized swimming and sinking speeds. These species thus also operate in a highly viscous regime at Reynolds numbers less than 100. These species thus experience both high frictional drag as well as pressure drag. Indeed, Vogel (2013) showed that the flow begins to separate around a circular cylinder (which is a good model of the shell shape of *H. inflatus*) at Reynolds numbers as low as 40. In addition, these species have a high pitching amplitude when swimming, a pattern which is facilitated by the coiled shell shape, which has low moment of inertia and low rotational drag (Murphy et al., 2016). This combination of translation and rotation used by coiled shell species may move the stagnation point on the shell to a different position (similar to the Magnus effect), thus increasing the lift to drag ratio. Coiled shell species that are sinking will presumably have a drag coefficient different from when they are swimming. At the sinking Reynolds numbers observed here, the wake behind an object in oncoming flow is symmetric, lacking

the Karman vortex street in an object's wake which would be present at higher *Re*. This presumably symmetric wake thus explains why the sinking trajectories of the coiled shell species are straight. It should be noted that the sinking pteropods recorded here sank with extended wings. Pteropods escaping with retracted wings would sink faster and at a higher *Re* (Gilmer and Harbison, 1986). For example, Bergan et al (2017) found that the coiled shell species *Limacina retroversa* in the size range of 0.56-2.37 mm sank at speeds of 16-19 mm/s with wings withdrawn and speeds of 13-16 mm/s with wings extended. These sinking values are similar those of the coiled shell thecosome species studied here (Table 2).

The elongated shell pteropods have larger shells and swim at speeds slightly faster than the coiled shell species, thus resulting in normalized swimming speeds an order of magnitude lower than the coiled shell species. The elongated shell species thus operate at a Reynolds number an order of magnitude higher (100-600) than that of the coiled shell species. Pressure drag is thus more important for the elongated shell pteropods at this *Re* as compared to the coiled shell species. Similar to the coiled shell species, the elongated shell species also exhibit forward-backwards body pitching with every wing stroke, but the pitching amplitude seems to be less for the elongated shell species. For example, Karakas et al. (2020) showed that *C. atlantica* has a pitching angle of 25°, which is much less than pitching amplitudes previously measured for the coiled shell species *L. helicina* (up to 60°) and *L. helicina antarctica* (up to 110°; Murphy et al 2016, Adhikari et al 2016). The lower pitching amplitude of the elongated shell species makes sense because these shells have greater rotational drag and rotational inertia as compared to coiled shells. The elongated shell thecosomes are larger and weigh more and are generally less maneuverable than the coiled shell thecosomes, likely because rotational and translational acceleration theoretically can be scaled as $\text{mass}^{-2/3}$ and $\text{mass}^{-1/3}$ respectively (Vogel, 1988; Dudley, 2002). Inside the elongated shell group, there are also large differences in maneuverability. For example, though *H. striata* and *S. subula* have similarly shaped shells, the shell of *H. striata* seems more delicate, corresponding with its greater swimming over *S. subula*. Similarly, *C. atlantica*, with its large shell, is the least maneuverable of the elongated shell thecosomes. The higher swimming speeds and maneuverability of some species could be one reason why they are less sampled in net tows.

The sinking behavior (e.g. glide angle, trajectory, stability) of the various species depends on factors including size, shell shape, and the relative locations of the center of mass (center of gravity) and the geometric center (center of buoyancy). Indeed, in a study of the sinking behavior of simple cylindrical shapes, Chu et al. (2005) found that the relative locations of the center of mass and center of geometry largely controlled sinking trajectory and orientation and that a larger offset between these two points resulted in less lateral travel while sinking. However, in general, the descent angle cannot be predicted from this offset because instantaneous hydrodynamic forces (e.g. lift, drag, vortices created by flow past the object) could impact the trajectory (Chu et al., 2005), and the relative importance of these fluid forces increase with the Reynolds number. In considering pteropod shells, non-uniform mass distributions (e.g. differences in shell thickness) and complex geometries (e.g. changing wing positions) make knowledge of the locations of the center of mass and the geometric center extremely difficult. Nonetheless, we suspect that the coiled species, which sink at a low Re, always have their center of mass located below their geometric center (which includes the wings), and this may explain their stability and steep angle of descent while sinking. In contrast, elongated shell species may either rotate towards a horizontal orientation with the wings outstretched (e.g. *C. atlantica*) or may sink in a vertical position with the wings held upwards in a streamlined position (e.g. *H. striata* and *S. subula*). These different

orientations will differentially affect the coefficient of drag. The species *C. atlantica* is larger than the other elongated species and thus may energetically benefit from a larger coefficient of drag resulting from its more horizontal sinking position, which slows its sinking (Field et al., 1997; Amin et al., 2019). For those elongated species that tend to rotate to a horizontal position while sinking, we suspect that their center of mass is located close to or above their geometric center. In addition, an order of magnitude increase in sinking *Re* from the coiled shell species to the elongated shell species also plays an important role in shell reorientation as the boundary layer separation starts to occur in this *Re* (10^2) regime and the resulting drag and lift forces introduce a non-negligible deflecting moment which alters the animal's trajectory, thus corresponding to the higher glide angles found for these species as a group. Further, Chamberlain and Weaver (1978) theoretically showed that sinking behavior is largely controlled by shell geometry. This finding also is observed in our study as the sinking behavior of these pteropod species naturally grouped by shell geometry.

The globular shell shape species *D. trispinosa* has the largest shell size among the thecosome groups studied here. It also appears to be a strong swimmer as well. This globular shell species operates at a Reynolds number an order of magnitude higher (700-1600) than that of the elongated shell species and two orders of magnitude greater than coiled ones. These *Re* numbers represent the upper limit of the intermediate *Re* regime, where both inertia and viscosity are important, and the lower end of the *Re* regime where inertia effects dominate. The pressure drag is thus dominant for the globular shell pteropods at this *Re* as compared to the coiled shell species and elongated shell species. Distinct from the coiled shell and elongated shell species, this globular shell species does not exhibit forward-backwards body pitching with each half wing stroke. Instead, the dorso-ventrally flattened shell of *D. trispinosa* appears to be adapted for lift generation as it has a large planform and the cross-sectional profile of a cambered airfoil. Indeed, unlike most of the coiled and elongated shell species, which swim almost vertically upwards with their shell hanging downwards like a pendulum, *D. trispinosa* species swims upward with an average climbing angle of 47.5±8.7°. This characteristic shell orientation thus likely allows the shell to generate lift which would aid its ascent. With its high lift generation capability *D. trispinosa* has a high maneuverability compared to other thecosome groups. When sinking, this globular shell species glides with its wings partially folded. Considering the relatively high Reynolds number regime at which *D. trispinosa* sinks, it likely benefits from the large flat surface area that the shell provides, thus slowing down the sinking rate in the water column. The lift force on the flat shell and wings of the globular species may also cause greater horizontal deviation in their downward trajectories, a pattern which matches the higher glide angles observed for the *D. trispinosa,* since the shell shape is more aerodynamically streamlined and is always observed to orient in a horizontal position which maximizes the projected area in the sinking direction. Finally, it should be noted that there is only one globular species analyzed here which may not be fully representative of the globular shell shaped group which are often less dorsoventrally compressed. More species need to be studied to reach more representative results.

As seen in Table 2, *Pneumoderma atlantica* studied here is larger than its co-occurring thecosome species except for *D. trispinosa*, which is the same size. Further, the swimming speed of *P. atlantica* is less than the swimming speeds of these thecosomes. These low swimming speeds reflect the fact that *P. atlantica*, without external disturbance in the lab environment, spent most of its time hovering or slowly translating in a small area.

Pneumoderma atlantica can hover for an extended amount of time partly because the lack of heavy calcareous shells, which make these animal less negatively buoyant. Though fast-swimming escape or hunting behaviors were not observed here, it has been reported that some gymnosome species can swim as fast as 1000 mm s^{-1} for short time intervals (Hamner et al., 1975; Lalli and Gilmer, 1989), resulting in high Reynolds numbers comparable to that of fast-swimming fishes and some flying birds (*Re*=10,000). Thus, their streamlined body shape, which is more efficient because of the low drag coefficient this body geometry provides in this *Re* regime, is advantageous for gymnosomes. Further, all gymnosomes studied to date have wings with short wingspans and low aspect ratios as compared to the thecosome pteropods. These low aspect ratio wings are useful for generating high levels of thrust and acceleration, which are useful for the quick maneuvers necessary for these predators to capture thecosomes. Interestingly, though of comparable body length with the temperate gymnosome species *C. limacina* and the polar species *C. antarctica* (Satterlie et al., 1985; Borrell et al., 2005; Szymik and Satterlie, 2011), the warm water species *P. atlantica* studied here has larger wingbeat frequency than its cold water counterparts. Other researchers have found that flies reared at high temperatures have lower body mass and smaller wings and exhibit higher beat frequencies than those reared at low temperatures, a trend related to the decreased wing loading and resonance and increased wing moment of inertia and induced power requirements to move larger wings (Barnes and Laurie-Ahlberg, 1986; Pétavy et al., 1997; Lehmann, 1999; Dillon and Dudley, 2004; Frazier et al., 2008). It is not known how the wing surface area compares among polar and tropical gymnosome species. In addition, water viscosity likely plays an important role in modulating flapping frequency since the kinematic viscosity of seawater changes greatly between polar and tropical temperatures.

The atlantiid heteropods studied here are larger than the coiled shell thecosomes but smaller than the elongated and globular shell thecosomes. Further, though they have a distinct body geometry and swimming style (Karakas et al., 2018), these heteropods have comparable swimming speeds to all but the fastest swimming thecosomes. It is known that atlantiid heteropods are visual predators and have large, complex eyes with a narrow retina and narrow field of view which they may actively rotate up and down through a 90° arc to scan the surrounding environment for prey (Seapy, 1980; Land, 1982, 1999). However, there is disagreement in the literature regarding their prey, with Thiriot-Quievreux (1973) and Lalli and Gilmer (1989) suggesting that thecosomes are primary prey and Wall-Palmer (2016) suggesting otherwise using fossil evidence. Based on the swimming speeds and body sizes measured here, it seems possible that this small atlantiid heteropod would be capable of preying on small thecosomes in the coiled shell group such as *H. inflatus* and *L. bulimoides*. Larger thecosomes from the elongated and globular shell groups may be susceptible as prey to correspondingly larger atlantiid heteropods. Indeed, one such large unidentified atlantiid heteropod species (likely *Oxygyrus inflatus*) was observed preying on a *Clio pyramidata* while both were lying on the floor of an aquarium (Supplementary Movie S1).

The swimming and sinking characteristics described here will significantly bear on the diel vertical migration and vertical distributions of these marine snails. Figure 11 shows representative times needed to swim up or sink down 100 m in the water column. Upward swimming times and downward sinking times are based on the vertical component of the

average swimming speed and the vertical component of the average sinking speed, respectively. Both plots assume continuous sinking or swimming (i.e. no breaks in that behavior). The thecosome groups roughly follow a negative correlation of swimming time versus average body length, with the large globular species swimming that distance in about 40 minutes and small coiled species taking about 2 hours. In contrast, the sinking time has a strong negative relation with the average body length, with the large globular species sinking 100 m over about 20 minutes and the small coiled shell species taking 1.7 hours. Although this figure does not necessarily represent the real distance across which these marine snails migrate or the time required for that migration, it gives insight into their vertical distribution in the water column and into the energy required for diel vertical migration. Larger species sink down and swim up much faster and thus can be active at much greater depths whereas the slower and smaller species are limited to shallower depths.

Besides its relevance to maintenance of vertical habitat, predator/prey interactions and migratory behavior, the rate of thecosome pteropod sinking is biogeochemically important as shells from dead thecosome sink to the deep ocean and dissolve in high pressure, contributing an estimated 12-13% of the carbonate flux globally (Berner and Honjo, 1981; Tsurumi et al., 2005) and greater than 50% of the carbonate flux in the Southern Ocean (Hunt et al., 2008). The sinking rates measured here, although likely slower than that of dead or empty shells, give insight into how shell size may affect carbon flux rate. These findings may be important as we seek to understand changes to flux due to anthropogenic forcings. Using time series observations, shifts in planktonic community composition, including pole-ward movement of centers of abundance have been demonstrated (Southward et al., 1995; Oviatt, 2004; Mackas et al., 2007) including in pteropods (Beaugrand et al., 2012) . Due to basic thermodynamic principles, warmer conditions tend to be more favorable for smaller species and smaller individuals within a species (Berger, 1978; Berner and Honjo, 1981; Almogi-Labin et al., 1988; Fabry, 1990; Fabry and Deuser, 1991; Daufresne et al., 2009). Not only do smaller individuals carry less carbonate to depth, but our results demonstrate that they also sink slower, providing a greater window of time for dissolution effects to reduce the vertical extent of their carbonate export. Thus, changes in the species or size class composition could reduce both the amount and depth of calcium carbonate export. Ocean acidification, which degrades fragile aragonite shells and reduces calcification, may additionally alter these sinking rates, as well as pteropod swimming and sinking behavior, in the future (Sabine et al., 2004; Manno et al., 2010; Orr, 2011; Chang and Yen, 2012; Comeau et al., 2012; Adhikari et al., 2016; Murphy et al., 2016; Bergan et al., 2017; Bednaršek et al., 2019).

Body length has previously been analyzed as a predictor for vertical migration extent based on the idea that migration is a balance between the energetics of swimming and the ability of an individual to hide from visual predators. These constraints both scale with size, but in opposite directions. Consequently, it has been demonstrated that there is a U-shaped curve to the extent of vertical migration for copepods in the California current (Ohman and Romagnan, 2016), with both longer and shorter individuals having small migrations, and intermediate sized organisms migrating the most. Longer individuals in the study by Ohman and Romagnan (2016) had a deeper overall habitat, while shorter individuals were present higher in the water column. Our dataset has substantially less sampling, however, the preferred depth habitat patterns are consistent with these previous findings. Longer species

>7mm tended to have deeper distributions (*C. atlantica*, *D. trispinosa*, *Pneumoderma atlantica*), while smaller species < 3 mm (*H. inflatus, L. bulimoides*) are found abundantly in the upper water column (Supplementary Figure S4A). However, the vertical extent of migration patterns of the pteropods analyzed here do not have the same U-shaped curve, with some of the smaller species having long migrations (*H. inflatus;* 200 m) and one of the larger species having the shortest migration (*C. clava*; 50 m). This suggests that for pteropods there are factors other than length driving migratory behavior. It is very likely that for the negatively buoyant pteropods shell morphology and mass play a bigger role than for the neutrally buoyant copepods. For example, *Creseis clava*, although quite long, is substantially less heavy than similarly sized individuals of other species owing to its needle like morphology, while *H. inflatus* is known to have a thinner and lighter shell than similarly sized Creseis species (Lalli and Gilmer, 1989).

Size does, however, play a strong role in the extent of migration within a species in our dataset, with longer individuals of *S. subula*, *C. clava*, *C. pyramidata*, and *H. inflatus* having substantially deeper distributions than smaller individuals of the same species. Ontogenetic partitioning of the water column has been observed previously in cephalopods, fish and crustaceans (i.e. Hunt and Seibel, 2000; Titelman and Fiksen, 2004; Maas et al., 2014), but has not previously been quantified in pteropods. The interplay between the energetics of vertical migration, the threat of visual predation and the size of an individual clearly strongly structure the habitat of pelagic species. Understanding these evolutionary constraints will only be possible with further analyses that interrogate migratory patterns by considering all of these factors with the addition of additional environmental parameters including prey availability, temperature and midwater oxygen.

CONCLUSIONS

In this paper, we studied the swimming and sinking kinematics, biomechanics, and depth distributions of a variety of warm water marine snail species, with a particular focus on how the shell shape, body geometry, and body size affect their locomotion from a fluid mechanics perspective. Among the thecosomes, the tiny coiled species, intermediate elongated species, and large globular shell species have distinct locomotion characteristics which correspond strongly with shell morphology and size. Swimming speeds, sinking speeds, and glide angles are positively correlated with shell size and thus also strongly depend on shell morphology, whereas small-scale oscillations in swimming trajectories are lower in the largest, globular species. These changes in locomotion characteristics tightly correspond to changes in the *Re* and the governing fluid dynamics, with *Re* increasing by an order of magnitude from the coiled shell species to the elongated shell species and again by another order of magnitude from the elongated shell species to the globular shell species. These differences in *Re* strongly affect the flow fields around the animal's wings and body and may point towards more recent lineages evolving shell shapes and swimming styles to produce better swimming performance by maximizing lift and minimizing drag. Speed of swimming does not, however, equate to the vertical extent of migration, emphasizing that other factors, likely including light, temperature, and predator and prey fields, have a strong influence on this ecologically important trait. Size does play a role in structuring the vertical habitat, with larger individuals tending to live deeper in the water column, while within a species, the extent of migration is greater in larger individuals.

Author Contributions

F.K., D.M., and A.M. conceived and designed the experiment. F.K. and D.M. carried out experimental work and data analysis. A.M. procured and identified the animals. F.K., D.M., and A.M. wrote the manuscript. J.W. helped digitize the videos. A.M and L.B-B. analyzed depth distributions. All authors approved the final manuscript.

Funding

Funding was provided by a National Science Foundation CAREER grant to D.W.M. (CBET #1846925), a grant from the National Academies of Science Keck Futures Initiative (NAKFI) to A.E.M and D.W.M, a University of South Florida (USF) New Researcher Grant to D.W.M, a USF Nexus Grant to D.W.M., and a Bermuda Institute of Ocean Sciences Grant in Aid to D.W.M. Distributional studies were funded through Simons Foundation International's BIOSSCOPE project (A.E.M and L.B-B.).

Acknowledgments

The authors gratefully acknowledge Kuvvat Garayev, Joseph Bello, Josh Arandia for assistance in collecting the animals and in conducting experiments, Paola Rossi Bruttini, Tristen Mee and Muhammad Shaikh for assistance with digitization, and Daniel D'Oliveira for assistance with creating 3D models. We appreciate the expertise and efforts of Hannah Gossner who assisted in the creation of the distributional plots.

Conflict of Interest

The authors declare that the research was conducted in the absence of any commercial or financial relationships that could be construed as a potential conflict of interest.

Supplementary Material

Supplementary File 1: MOCNESS net sampling methods.

Supplementary Table S1: Tukey-Kramer pairwise comparison test between the three pteropod shell shape groups. C - coiled shell, E – elongated shell, G – globular shell groups. Bold values show $P < 0.05$.

Supplementary Figure S1: Box plots of mean swimming speed, normalized mean swimming speed, sinking speed, and normalized mean sinking speed for three different shell shape groups. A) Mean swimming speed. B) Normalized mean swimming speed. C) Mean sinking speed. D) Normalized mean swimming speed plot. Groups which do not share a letter are statistically different from each other ($p < 0.05$) as determined by a one way ANOVA test and Tukey-Kramer pairwise comparisons. Outliers are demarcated as a plus sign (+).

Supplementary Figure S2: Swimming speed U of individual marine snails as a function of wing flapping frequency f for various marine snail species.

Supplementary Figure S3: Box plots of glide angle and swimming NGDR results for three different shell shape groups. A) Glide angle. B) NGDR. Groups which do not share a letter are statistically different from each other ($p < 0.05$) as determined by a one way ANOVA test and Tukey-Kramer pairwise comparisons. Outliers are demarcated as a plus sign (+).

Supplementary Figure S4: Vertical distributions based on image data and molecular data. A) Day and Night vertical distribution based on the relative proportion of the population within a particular size bin (mm). B) Average day and night biomass profiles based on imaging. C) Average day and night biomass profiles based on molecular barcoding.

Supplementary Movie S1: Video of a large unidentified atlantiid heteropod species (likely *Oxygyrus inflatus*) preying on the pteropod *Clio pyramidata* while both were lying on the floor of an aquarium. Video shakiness was removed by using Warp Stabilizer effect in Adobe Premiere Pro CC 2018.

872 **REFERENCES**

873 Adhikari, D., Webster, D. R., and Yen, J. (2016). Portable tomographic PIV measurements of
874 swimming shelled Antarctic pteropods. *Exp. Fluids* 57, 1–17. doi:10.1007/s00348-016-
875 2269-7.

876 Almogi-Labin, A., Hemleben, C., and Deuser, W. G. (1988). Seasonal variation in the flux of
877 euthecosomatous pteropods collected in a deep sediment trap in the Sargasso Sea. *Deep*
878 *Sea Res.* 35, 441464.

879 Amin, K., Huang, J. Mac, Hu, K. J., Zhang, J., and Ristroph, L. (2019). The role of shape-
880 dependent flight stability in the origin of oriented meteorites. *Proc. Natl. Acad. Sci. U. S.*
881 *A.* 116, 16180–16185. doi:10.1073/pnas.1815133116.

882 Amir, A., Daniel, M., Navas-Molina, J., Kopylova, E., Morton, J., Xu, Z. Z., et al. (2017).
883 Deblur rapidly resolves single-nucleotide community sequence patterns. *MSystems* 2, 1–
884 7.

885 Antezana, T. (2009). Species-specific patterns of diel migration into the Oxygen Minimum
886 Zone by euphausiids in the Humboldt Current Ecosystem. *Prog. Oceanogr.* 83, 228–
887 236. doi:10.1016/j.pocean.2009.07.039.

888 Barnes, P. T., and Laurie-Ahlberg, C. C. (1986). Genetic variability of flight metabolism in
889 Drosophila melanogaster. III. Effects of GPDH allozymes and environmental
890 temperature on power output. *Genetics* 112, 267–294.

891 Bé, A. W. H., and Gilmer, R. W. (1977). A zoogeographic and taxonomic review of
892 euthecosomatous Pteropoda. *Ocean. Micropaleontol.* 1, 773–808.

893 Beaugrand, G., Mcquatters-Gollop, A., Edwards, M., and Goberville, E. (2012). Long-term
894 responses of North Atlantic calcifying plankton to climate change. *Nat. Clim. Chang.* 3,
895 263–267. doi:10.1038/nclimate1753.

896 Bednaršek, N., Feely, R. A., Howes, E. L., Hunt, B., Kessouri, F., León, P., et al. (2019).
897 Systematic review and meta-analysis towards synthesis of thresholds of ocean
898 acidification impacts on calcifying pteropods and interactions with warming. *Front.*
899 *Mar. Sci.* 6, 1–16. doi:10.3389/fmars.2019.00227.

900 Bednaršek, N., Možina, J., Vogt, M., O'Brien, C., and Tarling, G. A. (2012). The global
901 distribution of pteropods and their contribution to carbonate and carbon biomass in the
902 modern ocean. *Earth Syst. Sci. Data* 5, 167–186. doi:10.5194/essd-5-1-2013.

903 Bergan, A. J., Lawson, G. L., Maas, A. E., and Wang, Z. A. (2017). The effect of elevated
904 carbon dioxide on the sinking and swimming of the shelled pteropod *Limacina*
905 *retroversa*. *ICES J. Mar. Sci.* 74, 1893–1905. doi:10.1093/icesjms/fsx008.

906 Berger, W. H. (1978). Deep-sea carbonate: pteropod distribution and the aragonite
907 compensation depth. *Deep Sea Res.* 25, 447–452.

908 Berner, R. A., and Honjo, S. (1981). Pelagic Sedimentation of Aragonite: Its Geochemical
909 Significance. *Science (80-.).* 211, 940–942.

910 Bianco, G., Mariani, P., Visser, A. W., Mazzocchi, M. G., and Pigolotti, S. (2014). Analysis
911 of self-overlap reveals trade-offs in plankton swimming trajectories. *J. R. Soc. Interface*
912 11. doi:10.1098/rsif.2014.0164.

913 Blanco-Bercial, L. (2020). Metabarcoding Analyses and Seasonality of the Zooplankton
914 Community at BATS. *Front. Mar. Sci.* 7, 1–16. doi:10.3389/fmars.2020.00173.

915 Borrell, B. J., Goldbogen, J. a, and Dudley, R. (2005). Aquatic wing flapping at low
916 Reynolds numbers: swimming kinematics of the Antarctic pteropod, *Clione antarctica*.
917 *J. Exp. Biol.* 208, 2939–2949. doi:10.1242/jeb.01733.

918 Buitenhuis, E. T., Le Quéré, C., Bednaršek, N., and Schiebel, R. (2019). Large Contribution
919 of Pteropods to Shallow CaCO3 Export. *Global Biogeochem. Cycles* 33, 458–468.
920 doi:10.1029/2018GB006110.

921 Burridge, A. K., Goetze, E., Wall-Palmer, D., Le Double, S. L., Huisman, J., and
922 Peijnenburg, K. T. C. A. (2017). Diversity and abundance of pteropods and heteropods
923 along a latitudinal gradient across the Atlantic Ocean. *Prog. Oceanogr.* 158, 213–223.
924 doi:10.1016/j.pocean.2016.10.001.

925 Chamberlain, J. A., and Weaver, J. S. (1978). Equations of motion for post-mortem sinking
926 of cephalopod shells. *J. Int. Assoc. Math. Geol.* 10, 673–689. doi:10.1007/BF01031898.

927 Chang, Y., and Yen, J. (2012). Swimming in the Intermediate Reynolds Range: Kinematics
928 of the Pteropod *Limacina helicina*. *Integr. Comp. Biol.* 52, 597–615.
929 doi:10.1093/icb/ics113.

930 Childress, S., and Dudley, R. (2004). Transition from ciliary to flapping mode in a swimming
931 mollusc: flapping flight as a bifurcation in Re. *J. Fluid Mech.* 498, 257–288.
932 doi:10.1017/S002211200300689X.

933 Chu, P. C., Gilles, A., and Fan, C. (2005). Experiment of falling cylinder through the water
934 column. *Exp. Therm. Fluid Sci.* 29, 555–568. doi:10.1016/j.expthermflusci.2004.08.001.

935 Comeau, S., Gattuso, J.-P., Nisumaa, A.-M., and Orr, J. (2012). Impact of aragonite
936 saturation state changes on migratory pteropods. *Proc. R. Soc. B Biol. Sci.* 279, 732–
937 738. doi:10.1098/rspb.2011.0910.

938 Daufresne, M., Lengfellner, K., and Sommer, U. (2009). Global warming benefits the small
939 in aquatic ecosystems. *Proc. Natl. Acad. Sci.* 106, 12788–12793.
940 doi:10.1073/pnas.0902080106.

941 Dillon, M. E., and Dudley, R. (2004). Allometry of maximum vertical force production
942 during hovering flight of neotropical orchid bees (Apidae: Euglossini). *J. Exp. Biol.* 207,
943 417–425. doi:10.1242/jeb.00777.

944 Dudley, R. (2002). Mechanisms and implications of animal flight maneuverability. *Integr.*
945 *Comp. Biol.* 42, 135–140. doi:10.1093/icb/42.1.135.

946 Fabry, V. J. (1990). Shell growth rates of pteropod and heteropod molluscs and aragonite
947 production in the open ocean: implications for the marine carbonate system. *J. Mar. Res.*
948 48, 209–222. doi:10.1357/002224090784984614.

949 Fabry, V. J., and Deuser, W. G. (1991). Aragonite and magnesian calcite fluxes to the deep
950 Sargasso Sea. *Deep Sea Res. Part A. Oceanogr. Res. Pap.* 38, 713–728.

951 Field, S. B., Klaus, M., Moore, M. G., and Nori, F. (1997). Chaotic dynamics of falling disks.
952 *Nature* 388, 252–254. doi:10.1038/40817.

953 Fonseca, V. G., Carvalho, G. R., Sung, W., Johnson, H. F., Power, D. M., Neill, S. P., et al.

(2010). Second-generation environmental sequencing unmasks marine metazoan biodiversity. *Nat. Commun.* 1. doi:10.1038/ncomms1095.

Frazier, M. R., Harrison, J. F., Kirkton, S. D., and Roberts, S. P. (2008). Cold rearing improves cold-flight performance in Drosophila via changes in wing morphology. *J. Exp. Biol.* 211, 2116–2122. doi:10.1242/jeb.019422.

Gilmer, R. W. (1972). Free-Floating Mucus Webs: A Novel Feeding Adaptation for the Open Ocean. *Science (80-.).* 176, 1239–1240.

Gilmer, R. W., and Harbison, G. R. (1986). Morphology and field behavior of pteropod molluscs: feeding methods in the families Cavoliniidae, Limacinidae and Peraclididae (Gastropoda: Thecosomata). *Mar. Biol.* 91, 47–57. doi:10.1007/BF00397570.

Gorsky, G., Ohman, M. D., Picheral, M., Gasparini, S., Stemmann, L., Romagnan, J. B., et al. (2010). Digital zooplankton image analysis using the ZooScan integrated system. *J. Plankton Res.* 32, 285–303. doi:10.1093/plankt/fbp124.

Hamner, W. M., Madin, L. P., Alldredge, A. L., Gilmer, R. W., and Hamner, P. P. (1975). Underwater observations of gelatinous zooplankton: Sampling problems, feeding biology, and behavior. *Limnol. Oceanogr.* 20, 907–917. doi:10.4319/lo.1975.20.6.0907.

Harbison, G. R., and Gilmer, R. W. (1992). Swimming, buoyancy and feeding in shelled pteropods: A comparison of field and laboratory observations. *J. Molluscan Stud.* 58, 337–339. doi:10.1093/mollus/58.3.337.

Hays, G. C. (2003). A review of the adaptive significance and ecosystem consequences of zooplankton diel vertical migrations. *Hydrobiologia* 503, 163–170. doi:10.1023/B:HYDR.0000008476.23617.b0.

Hedrick, T. L. (2008). Software techniques for two- and three-dimensional kinematic measurements of biological and biomimetic systems. *Bioinspir. Biomim.* 3, 034001. doi:10.1088/1748-3182/3/3/034001.

Howes, E. L., Bednaršek, N., Büdenbender, J., Comeau, S., Doubleday, A., Gallager, S. M., et al. (2014). Sink and swim: A status review of thecosome pteropod culture techniques. *J. Plankton Res.* 36, 299–315. doi:10.1093/plankt/fbu002.

Hunt, J. C., and Seibel, B. A. (2000). Life history of *Gonatus onyx* (Cephalopoda: Teuthoidea): Ontogenetic changes in habitat, behavior and physiology. *Mar. Biol.* 136, 543–552. doi:10.1007/s002270050714.

Hunt, B. P. V, Pakhomov, E. A., Hosie, G. W., Siegel, V., Ward, P., and Bernard, K. (2008). Pteropods in Southern Ocean ecosystems. *Prog. Oceanogr.* 78, 193–221. doi:10.1016/j.pocean.2008.06.001.

Jackson, B. E., Evangelista, D. J., Ray, D. D., and Hedrick, T. L. (2016). 3D for the people: multi-camera motion capture in the field with consumer-grade cameras and open source software. *Biol. Open* 5, 1334–1342. doi:10.1242/bio.018713.

Karakas, F., D'Oliveira, D., Maas, A. E., and Murphy, D. W. (2018). Using a shell as a wing: pairing of dissimilar appendages in atlantiid heteropod swimming. *J. Exp. Biol.* 221, jeb192062. doi:10.1242/jeb.192062.

Karakas, F., Maas, A. E., and Murphy, D. W. (2020). A novel cylindrical overlap-and-fling mechanism used by sea butterflies. *J. Exp. Biol.*, jeb.221499. doi:10.1242/jeb.221499.

996 Lalli, C. M., and Gilmer, R. W. (1989). *Pelagic snails: the biology of holoplanktonic*
997 *gastropod mollusks*. Stanford University Press.

998 Land, M. F. (1982). Scanning eye movements in a heteropod mollusc. *J. Exp. Biol.* 96, 427–
999 430.

1000 Land, M. F. (1999). Motion and vision: Why animals move their eyes. *J. Comp. Physiol. - A*
1001 *Sensory, Neural, Behav. Physiol.* 185, 341–352. doi:10.1007/s003590050393.

1002 Lehmann, F. O. (1999). Ambient temperature affects free-flight performance in the fruit fly
1003 Drosophila melanogaster. *J. Comp. Physiol. - B Biochem. Syst. Environ. Physiol.* 169,
1004 165–171. doi:10.1007/s003600050207.

1005 Lourakis, M. I., and Argyros, A. A. (2009). SBA: A software package for generic sparse
1006 bundle adjustment. *ACM Trans. Math. Softw.* 36, 2. doi:10.1145/1486525.1486527.

1007 Maas, A. E., Blanco-Bercial, L., and Lawson, G. L. (2013). Reexamination of the Species
1008 Assignment of Diacavolinia Pteropods Using DNA Barcoding. *PLoS One* 8.
1009 doi:10.1371/journal.pone.0053889.

1010 Maas, A. E., Frazar, S. L., Outram, D. M., Seibel, B. A., and Wishner, K. F. (2014). Fine-
1011 scale vertical distribution of macroplankton and micronekton in the Eastern Tropical
1012 North Pacific in association with an oxygen minimum zone. *J. Plankton Res.* 36, 1557–
1013 1575. doi:10.1093/plankt/fbu077.

1014 Maas, A. E., Wishner, K. F., and Seibel, B. A. (2012). Metabolic suppression in
1015 thecosomatous pteropods as an effect of low temperature and hypoxia in the eastern
1016 tropical North Pacific. *Mar. Biol.* 159, 1955–1967. doi:10.1007/s00227-012-1982-x.

1017 Mackas, D. L., Batten, S., and Trudel, M. (2007). Effects on zooplankton of a warmer ocean:
1018 Recent evidence from the Northeast Pacific. *Prog. Oceanogr.* 75, 223–252.
1019 doi:10.1016/j.pocean.2007.08.010.

1020 Manno, C., Morata, N., and Primicerio, R. (2012). *Limacina retroversa*'s response to
1021 combined effects of ocean acidification and sea water freshening. *Estuar. Coast. Shelf*
1022 *Sci.* 113, 163–171. doi:10.1016/j.ecss.2012.07.019.

1023 Manno, C., Tirelli, V., Accornero, A., and Fonda Umani, S. (2010). Importance of the
1024 contribution of *Limacina helicina* faecal pellets to the carbon pump in terra nova bay
1025 (Antarctica). *J. Plankton Res.* 32, 145–152. doi:10.1093/plankt/fbp108.

1026 Mohaghar, M., Adhikari, D., and Webster, D. R. (2019). Characteristics of swimming shelled
1027 Antarctic pteropods (*Limacina helicina antarctica*) at intermediate Reynolds number
1028 regime. *Phys. Rev. Fluids* 4, 1–10. doi:10.1103/PhysRevFluids.4.111101.

1029 Morton, J. E. (1954). The Biology of *Limacina Retroversa*. *J. Mar. Assess. U.K.* 3, 297–312.
1030 doi:10.1017/S002531540000833X.

1031 Murphy, D. W., Adhikari, D., Webster, D. R., and Yen, J. (2016). Underwater flight by the
1032 planktonic sea butterfly. *J. Exp. Biol.* 219, 535–543. doi:10.1242/jeb.129205.

1033 Ohman, M. D., and Romagnan, J. B. (2016). Nonlinear effects of body size and optical
1034 attenuation on Diel Vertical Migration by zooplankton. *Limnol. Oceanogr.* 61, 765–770.
1035 doi:10.1002/lno.10251.

1036 Orr, J. C. (2011). "Recent and future changes in ocean carbonate chemistry," in *Ocean*

acidification, 41–66.

Oviatt, C. A. (2004). The changing ecology of temperate coastal waters during a warming trend. *Estuaries* 27, 895–904.

Peijnenburg, K. T., Janssen, A. W., Wall-Palmer, D., Goetze, E., Maas, A., Todd, J. A., et al. (2019). The origin and diversification of pteropods predate past perturbations in the Earth's carbon cycle. *bioRxiv*, p.813386. doi:https://doi.org/10.1101/813386.

Pétavy, G., Morin, J. P., Moreteau, B., and David, J. R. (1997). Growth temperature and phenotypic plasticity in two Drosophila sibling species: Probable adaptive changes in flight capacities. *J. Evol. Biol.* 10, 875–887. doi:10.1007/s000360050059.

Ronquist, F., Teslenko, M., Van Der Mark, P., Ayres, D. L., Darling, A., Höhna, S., et al. (2012). Mrbayes 3.2: Efficient bayesian phylogenetic inference and model choice across a large model space. *Syst. Biol.* 61, 539–542. doi:10.1093/sysbio/sys029.

Sabine, C. C. L., Feely, R. R. A., Gruber, N., Key, R. M. R., Lee, K., Bullister, J. L., et al. (2004). The Oceanic Sink for Anthropogenic CO2. *Science (80-.).* 305, 367–371. doi:10.1126/science.1097403.

Satterlie, R. A., Labarbera, M., and Spencer, A. N. (1985). Swimming in the Pteropod Mollusk, *Clione Limacina* .1. Behavior and Morphology. *J. Exp. Biol.* 116, 189–204.

Schloss, P. D., Westcott, S. L., Ryabin, T., Hall, J. R., Hartmann, M., Hollister, E. B., et al. (2009). Introducing mothur: Open-source, platform-independent, community-supported software for describing and comparing microbial communities. *Appl. Environ. Microbiol.* 75, 7537–7541. doi:10.1128/AEM.01541-09.

Seapy, R. R. (1980). Predation by the epipelagic heteropod mollusk *Carinaria cristata* forma japonica. *Mar. Biol.* 60, 137–146. doi:10.1007/BF00389157.

Seuront, L., Brewer, M. C., and Strickler, J. R. (2004). "Quantifying Zooplankton Swimming Behavior: The Question of Scale," in *Handbook of Scaling Methods in Aquatic Ecology: Measurement, Analysis, Simulation*, 333–360.

Southward, A. J., Hawkins, S. J., and Burrows, M. T. (1995). Seventy years' observations of changes in distribution and abundance of zooplankton and intertidal organisms in the western English Channel in relation to rising sea temperature. *J. Therm. Biol.* 20, 127–155. doi:10.1016/0306-4565(94)00043-I.

Stamatakis, A. (2014). RAxML version 8: A tool for phylogenetic analysis and post-analysis of large phylogenies. *Bioinformatics* 30, 1312–1313. doi:10.1093/bioinformatics/btu033.

Szymik, B. G., and Satterlie, R. a (2011). Changes in wingstroke kinematics associated with a change in swimming speed in a pteropod mollusk, *Clione limacina*. *J. Exp. Biol.* 214, 3935–47. doi:10.1242/jeb.058461.

Thabet, A. A., Maas, A. E., Lawson, G. L., and Tarrant, A. M. (2015). Life cycle and early development of the thecosomatous pteropod *Limacina retroversa* in the Gulf of Maine, including the effect of elevated CO2 levels. *Mar. Biol.* 162, 2235–2249. doi:10.1007/s00227-015-2754-1.

Thiriot-Quiévreux, C. (1973). Heteropoda. *Ocean. Mar. Biol. Ann. Rev* 11, 237–261.

Titelman, J., and Fiksen, Ø. (2004). Ontogenetic vertical distribution patterns in small

copepods: Field observations and model predictions. *Mar. Ecol. Prog. Ser.* 284, 49–63. doi:10.3354/meps284049.

Tsurumi, M., Mackas, D. L., Whitney, F. A., Dibacco, C., Galbraith, M. D., and Wong, C. S. (2005). Pteropods , eddies , carbon flux , and climate variability in the Alaska Gyre. *Deep Sea Res. Part II Top. Stud. Oceanogr.* 52, 1037–1053. doi:10.1016/j.dsr2.2005.02.005.

Vandromme, P., Lars, S., Garcìa-Comas, C., Berline, L., Sun, X., and Gorsky, G. (2012). Assessing biases in computing size spectra of automatically classified zooplankton from imaging systems: A case study with the ZooScan integrated system. *Methods Oceanogr.* 1–2, 3–21. doi:10.1016/j.mio.2012.06.001.

Vogel, S. (1988). *Life's devices: the physical world of animals and plants*. Princeton University Press.

Vogel, S. (2013). *Comparative biomechanics: life's physical world*. Princeton University Press.

Wall-Palmer, D., Metcalfe, B., Leng, M. J., Sloane, H. J., Ganssen, G., Vinayachandran, P. N., et al. (2018). Vertical distribution and diurnal migration of atlantid heteropods. *Mar. Ecol. Prog. Ser.* 587, 1–15. doi:10.3354/meps12464.

Wall-Palmer, D., Smart, C. W., Kirby, R., Hart, M. B., Peijnenburg, K. T. C. A., and Janssen, A. W. (2016). A review of the ecology, palaeontology and distribution of atlantid heteropods (Caenogastropoda: Pterotracheoidea: Atlantidae). *J. Molluscan Stud.* 82, 221–234. doi:10.1093/mollus/eyv063.

Wiebe, P. H., Morton, A. W., Bradley, A. M., Backus, R. H., Craddock, J. E., Barber, V., et al. (1985). New development in the MOCNESS, an apparatus for sampling zooplankton and micronekton. *Mar. Biol.* 87, 313–323. doi:10.1007/BF00397811.

Wormelle, R. L. (1962). A Survey of the Standing Crop of Plankton of the Florida Current.VI. A Study of the Distribution of the Pteropods of the Florida Current. *Bull. Mar. Sci.* 12, 95–136.

Wormuth, J. H. (1981). Vertical distributions and diel migrations of Euthecosomata in the northwest Sargasso Sea. *Deep Sea Res. Part A, Oceanogr. Res. Pap.* 28, 1493–1515. doi:10.1016/0198-0149(81)90094-7.

Zhou, Z., and Mittal, R. (2017). Swimming without a Spine: Computational Modeling and Analysis of the Swimming Hydrodynamics of the Spanish Dancer. *Bioinspir. Biomim.* 13, p.015001. doi:10.1088/1748-3190/aa9392.

Zhou, Z., and Mittal, R. (2018). Swimming performance and unique wake topology of the sea hare (*Aplysia*). *Phys. Rev. Fluids* 3, 33102. doi:10.1103/PhysRevFluids.3.033102.

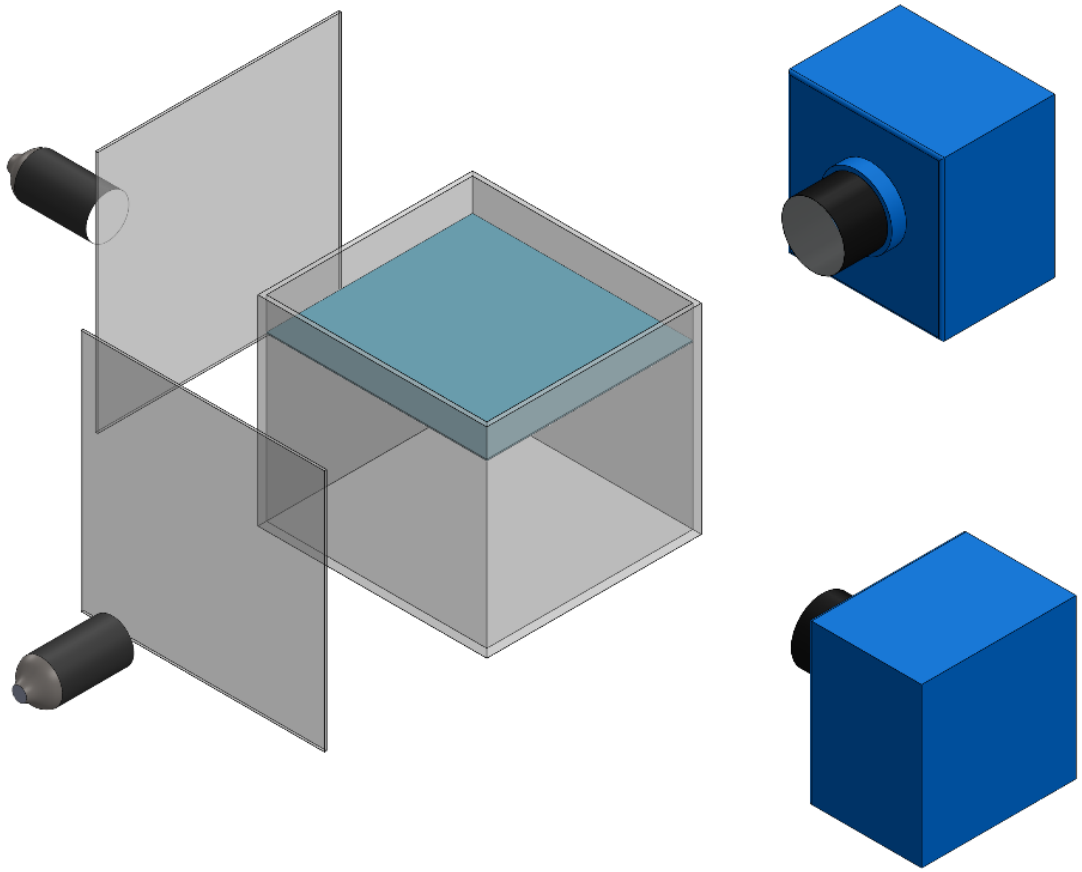

Figure 1: Schematic of low magnification stereophotogrammetry system using to record swimming trajectories of various marine snails

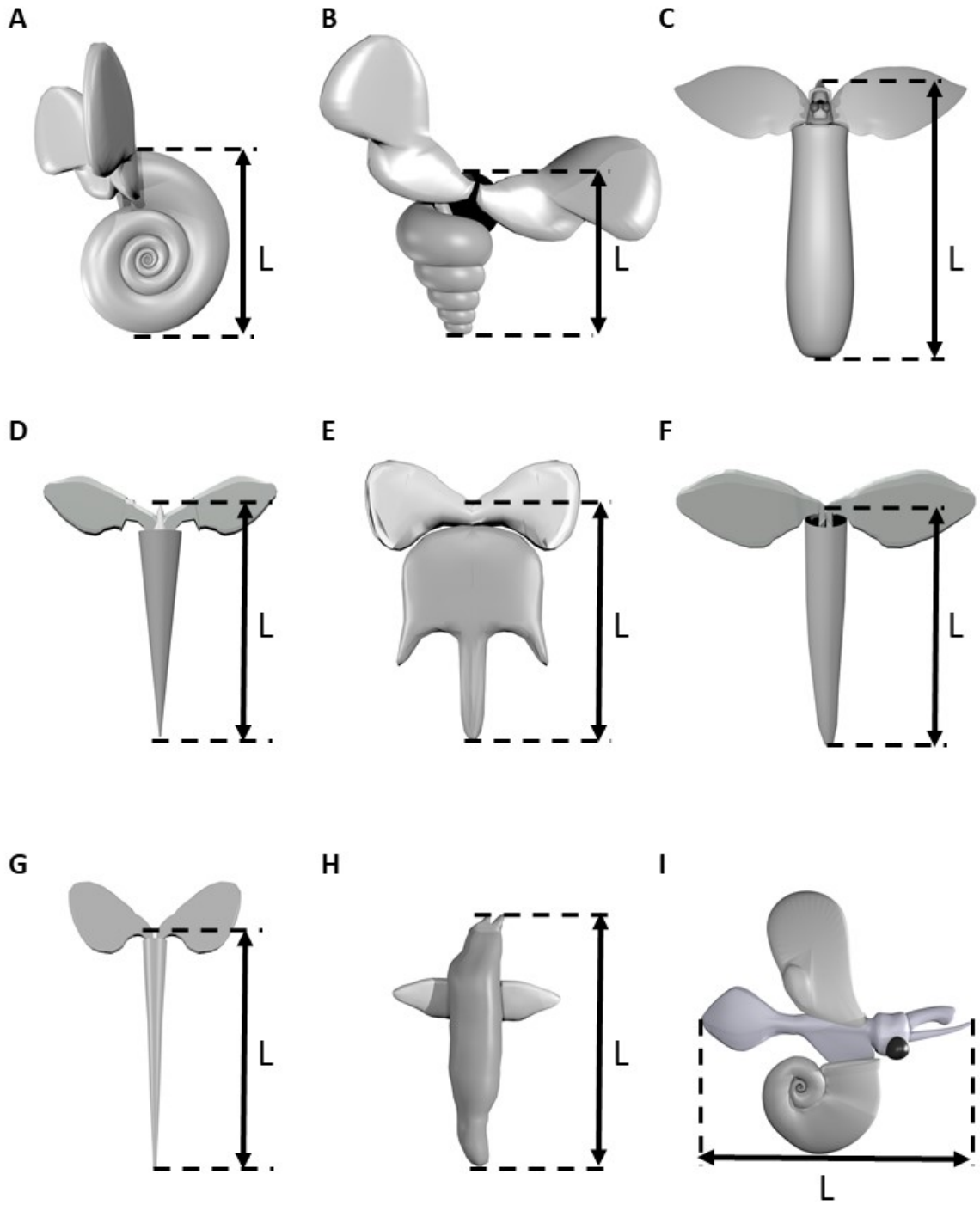

Figure 2: Three-dimensional models of various marine snail species. A) *Heliconoides inflatus*, B) *Limacina bulimoides*, C) *Cuvierina atlantica*, D) *Hyalocylis striata*, E) *Diacria trispinosa*, F) *Styliola subula*, G) *Creseis clava*, H) *Pneumoderma atlantica*, I) Heteropod sp. Models are not drawn to scale.

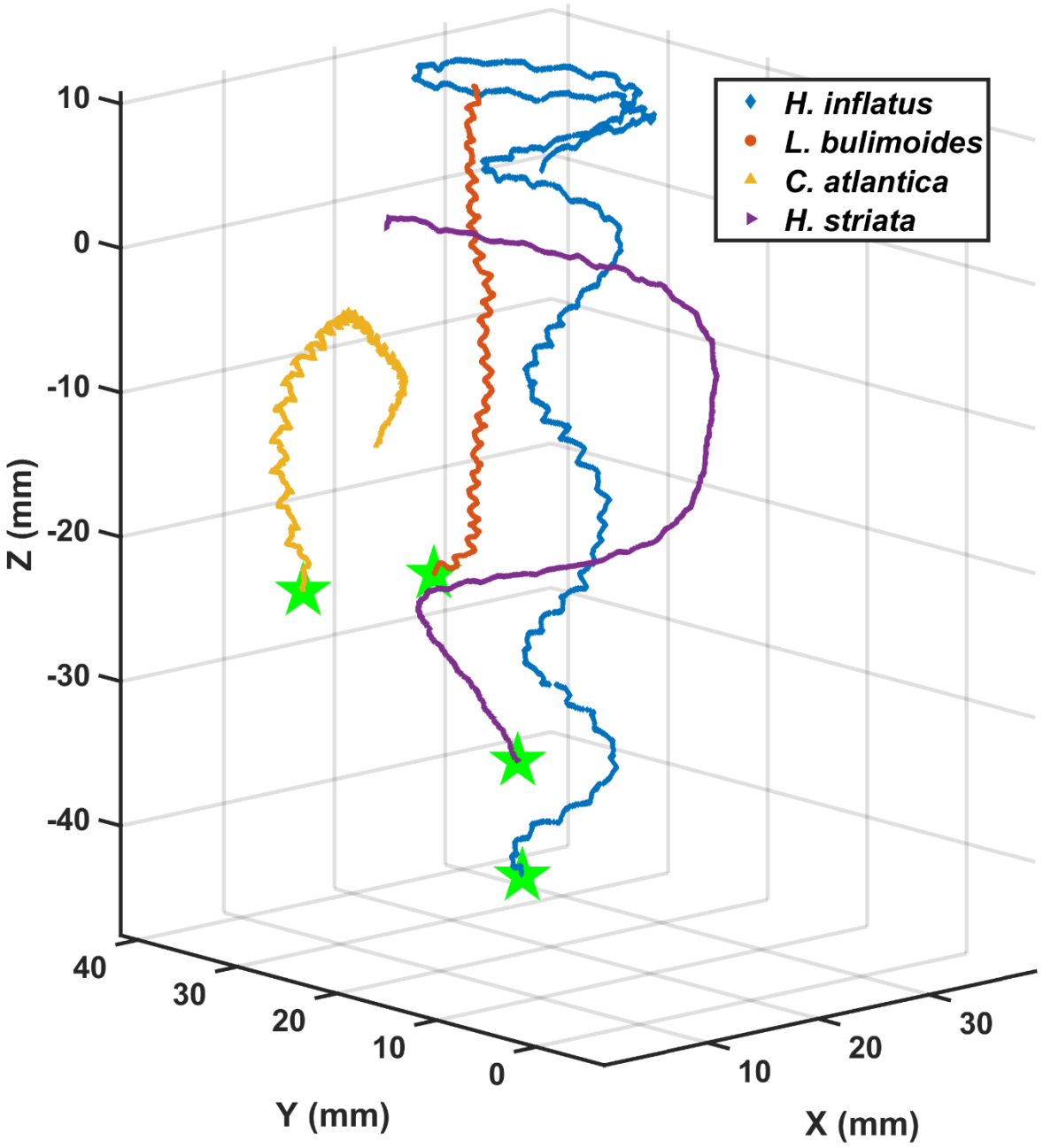

Figure 3: Three-dimensional upward swimming trajectories of four thecosomatous pteropod species.

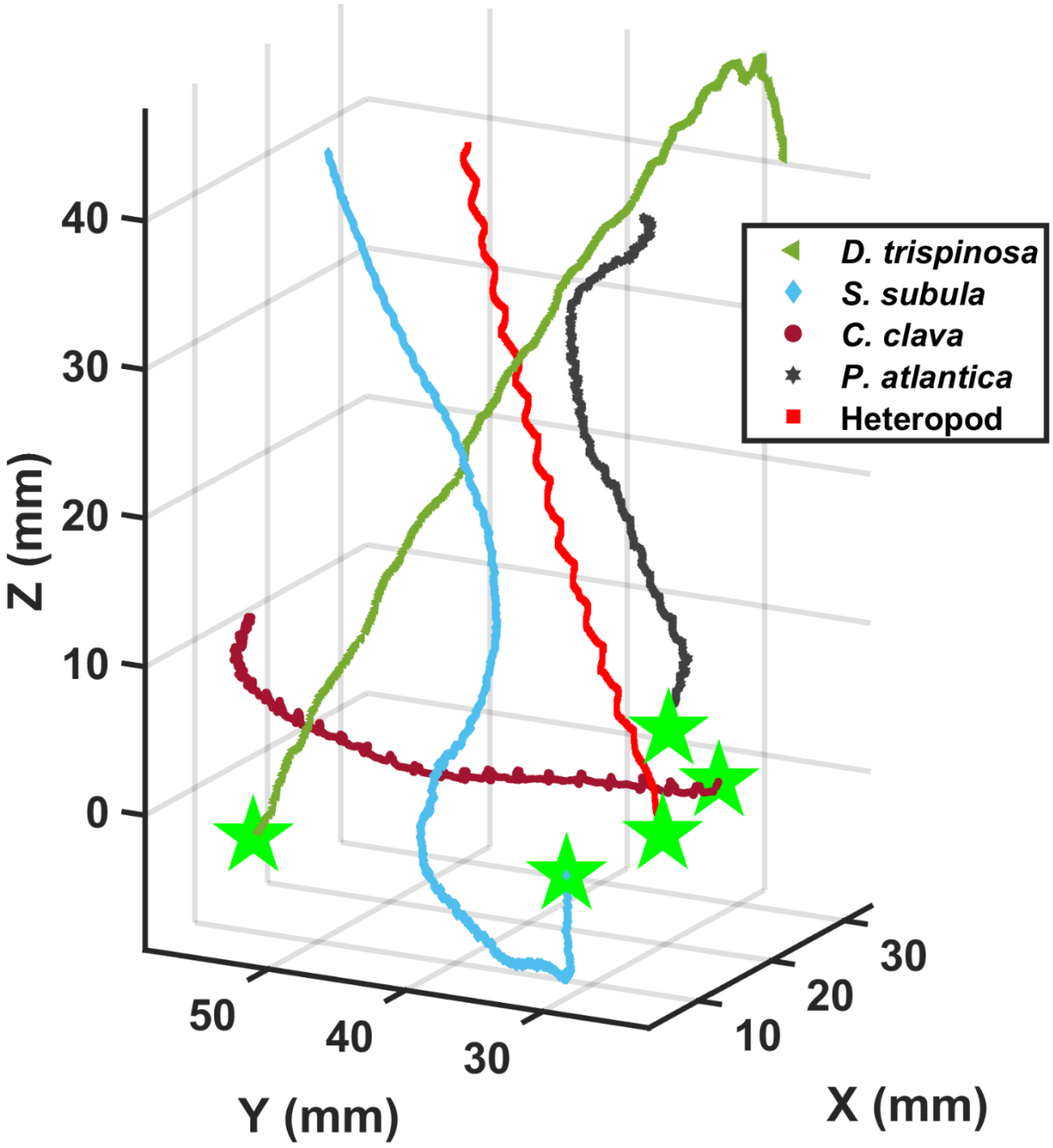

Figure 4: Three-dimensional upward swimming trajectories of three thecosomatous pteropod species, one gymnosomatous pteropod species, and one atlantiid heteropod species.

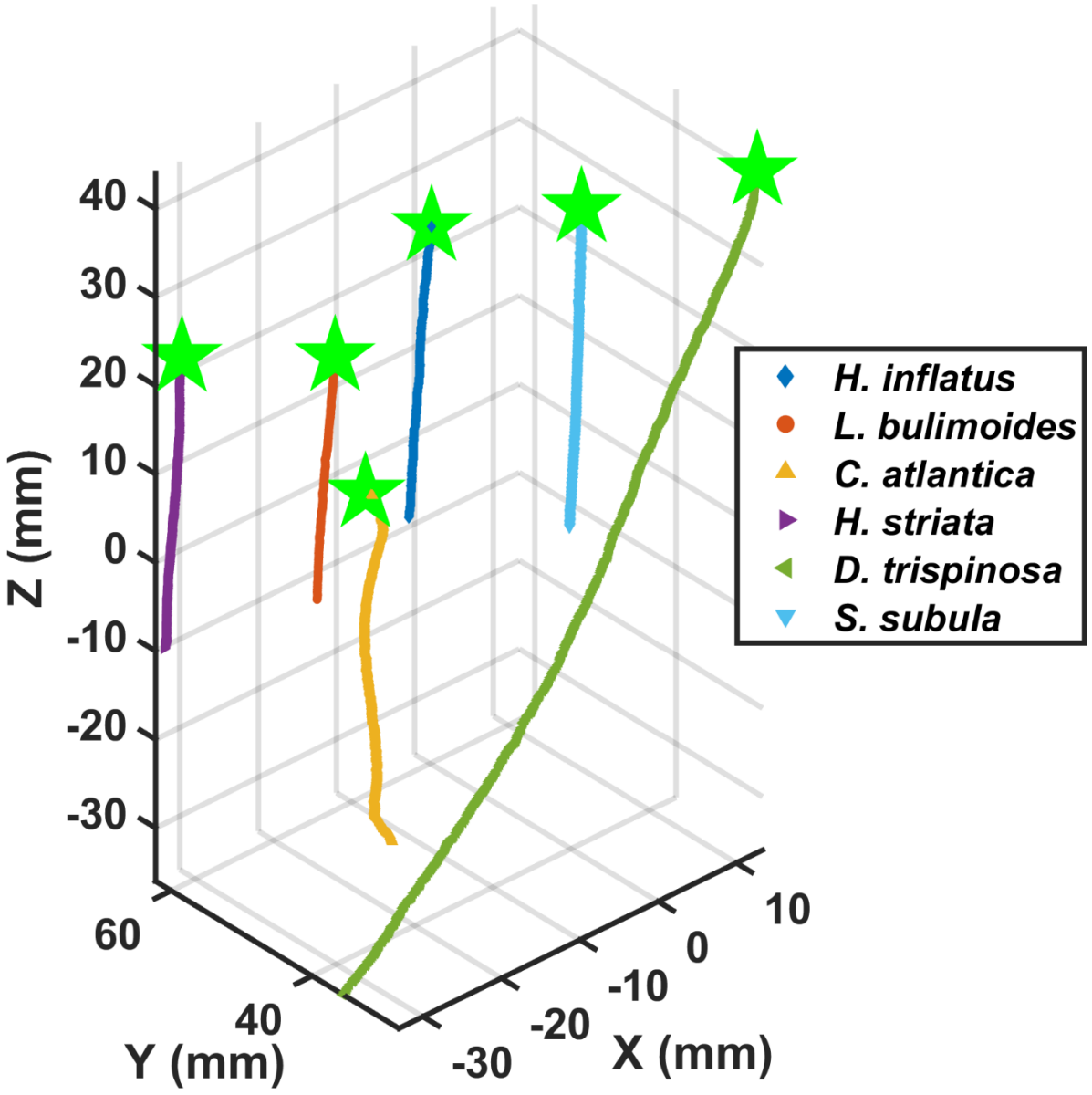

Figure 5: Three-dimensional downward sinking trajectories of six thecosomatous pteropod species.

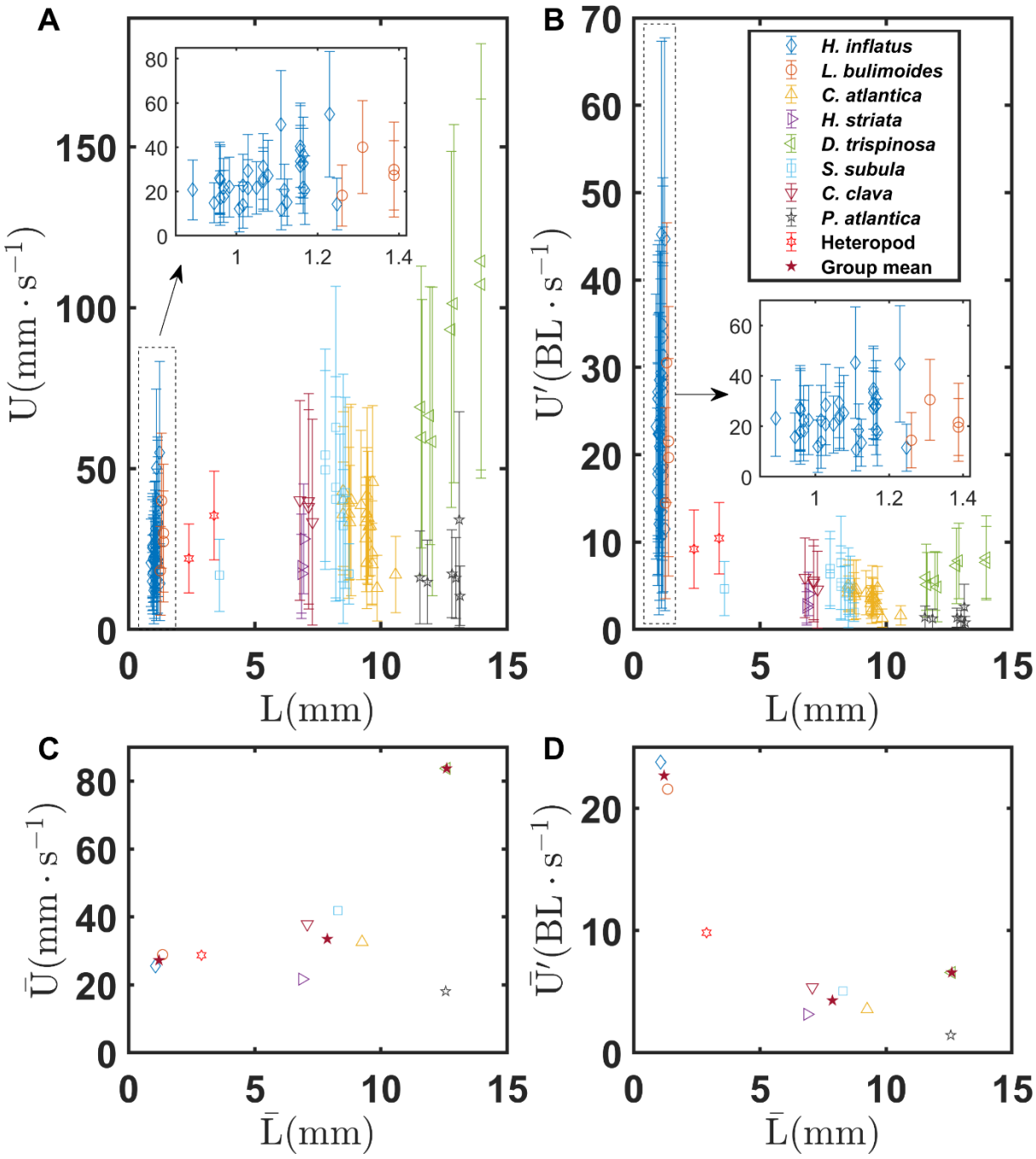

Figure 6: A) Mean and standard deviation of swimming speed U of individual marine snails as a function of body length L for various marine snail species. B) Normalized mean and standard deviation of swimming speed U' of individual marine snails as a function of body length L for various marine snail species. C) Mean swimming speed $\bar{U}$ of various marine snail species as a function of mean body length $\bar{L}$. D) Mean swimming speed $\bar{U}'$ of various marine snail species as a function of mean body length $\bar{L}$. Stars in C) and D) indicate group means of coiled, elongated, and globular shelled thecosome species.

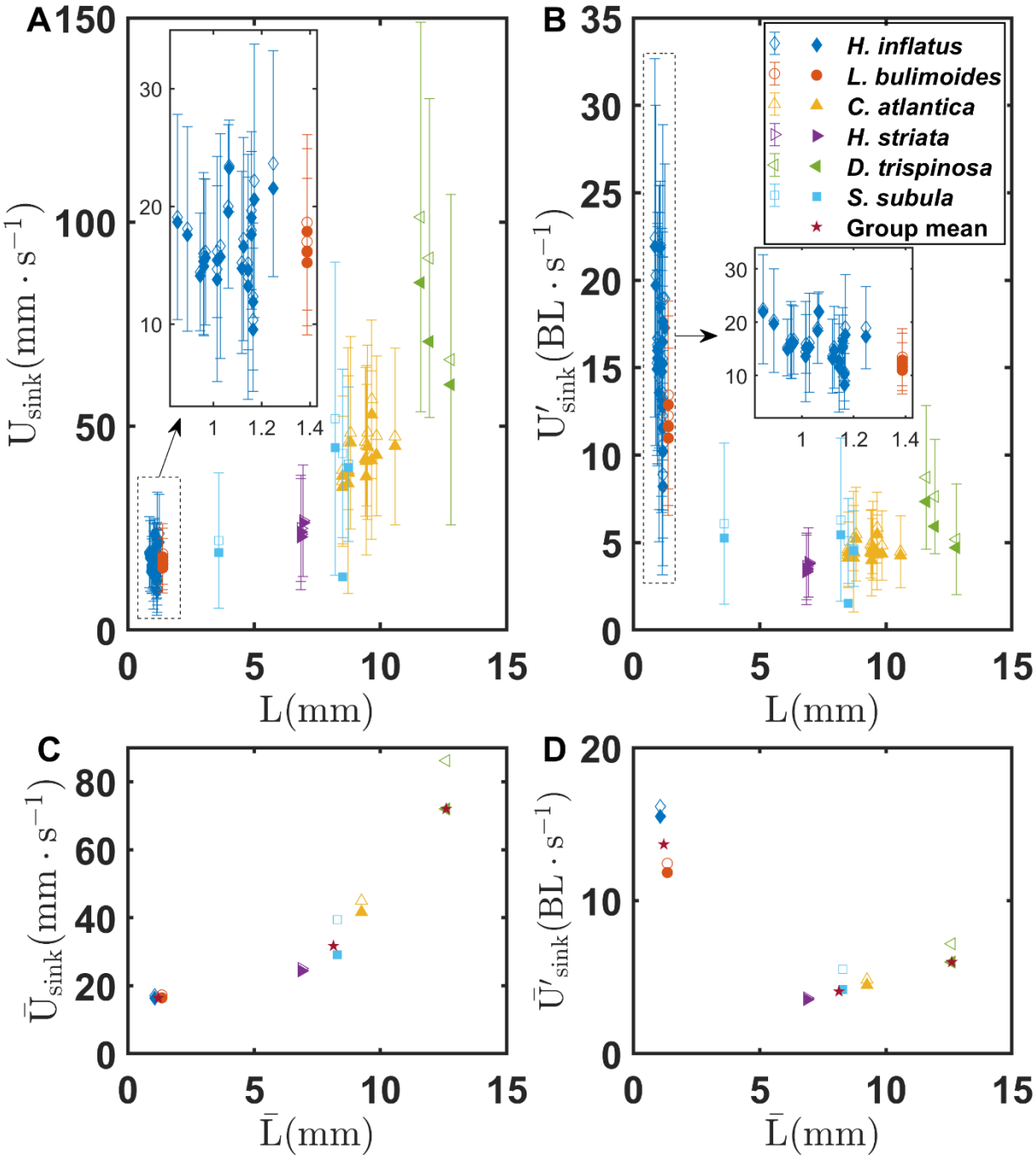

Figure 7: A) Mean and standard deviation of sinking speed U_{sink} of individual marine snails as a function of body length L for various marine snail species. B) Normalized mean and standard deviation of sinking speed U'_{sink} of individual marine snails as a function of body length L for various marine snail species. C) Mean sinking speed $\bar{U}_{sink}$ of various marine snail species as a function of mean body length $\bar{L}$. D) Mean sinking speed $\bar{U}'_{sink}$ of various marine snail species as a function of mean body length $\bar{L}$. Stars in C) and D) indicate group means of coiled, elongated, and globular shelled thecosome species.

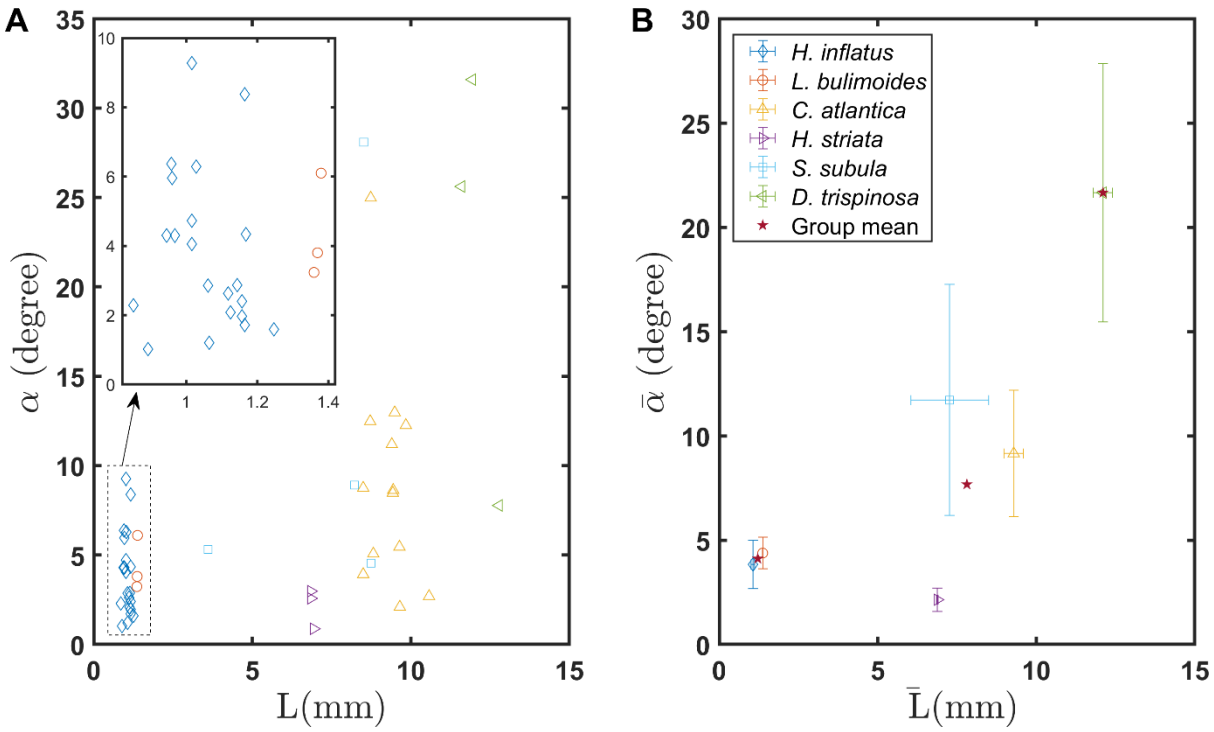

Figure 8: A) Gliding angle of individual marine snails as a function of body length L, B) Mean gliding angles of various marine snail species as a function of mean body length $\bar{L}$. Stars in B) indicate group means of coiled, elongated, and globular shelled thecosome species.

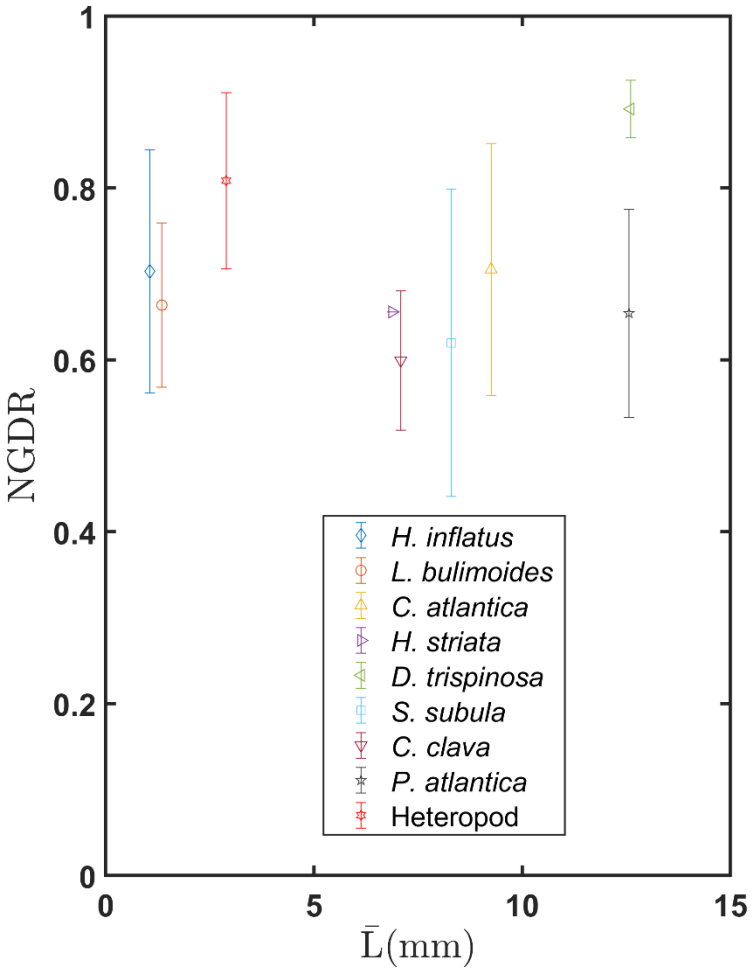

Figure 9: Mean and standard deviation of NGDR measured over five body lengths for various marine snail species as a function of mean body length $\bar{L}$.

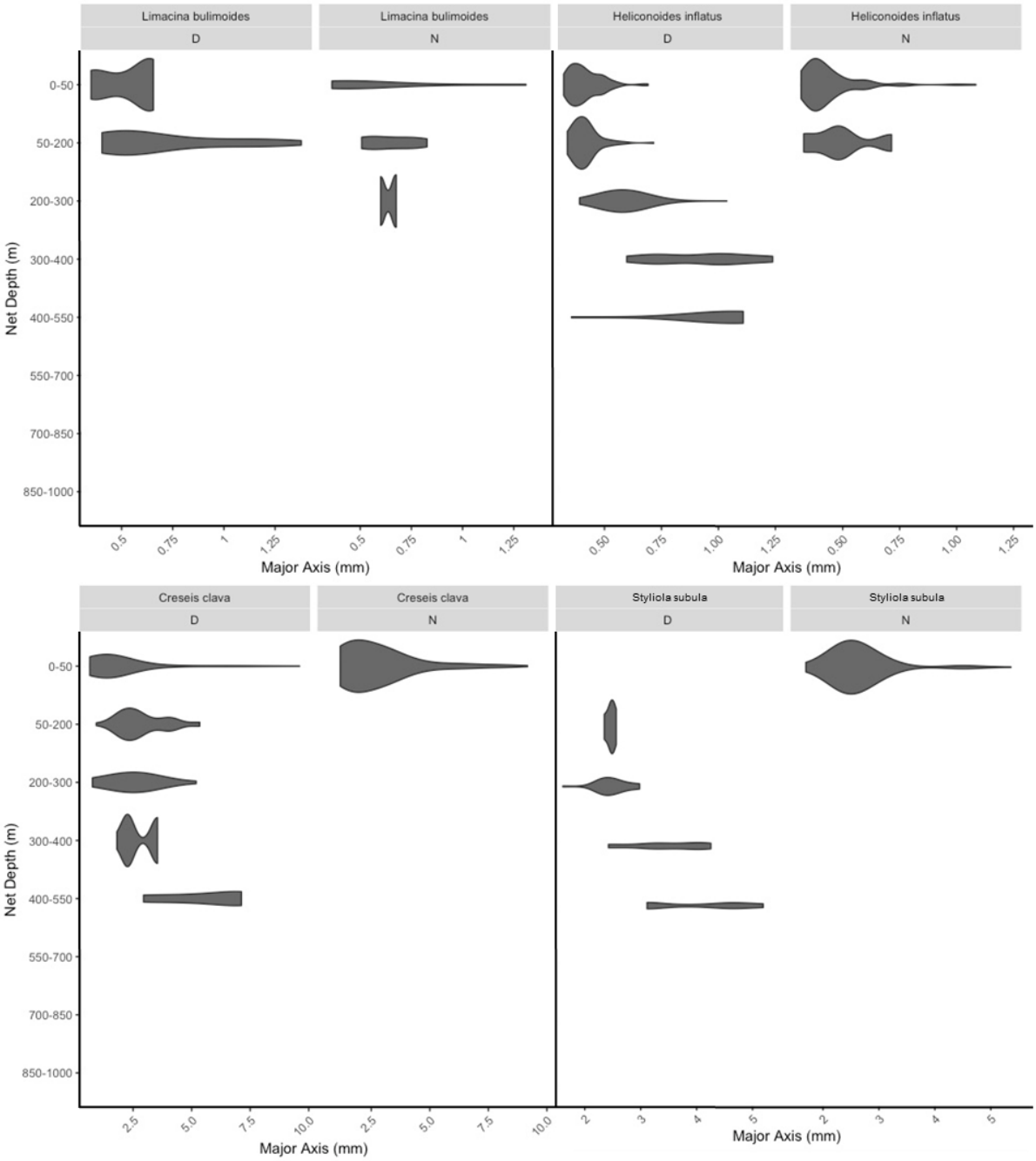

Figure 10: Day and Night vertical distribution of species from MOCNESS net image data. The length of the organisms (x-axis) is plotted versus the median depth of the net of collection (y-axis) to demonstrate size-based differences in habitat selection. The width of the bar corresponds to relative abundance of individuals in that size bin.

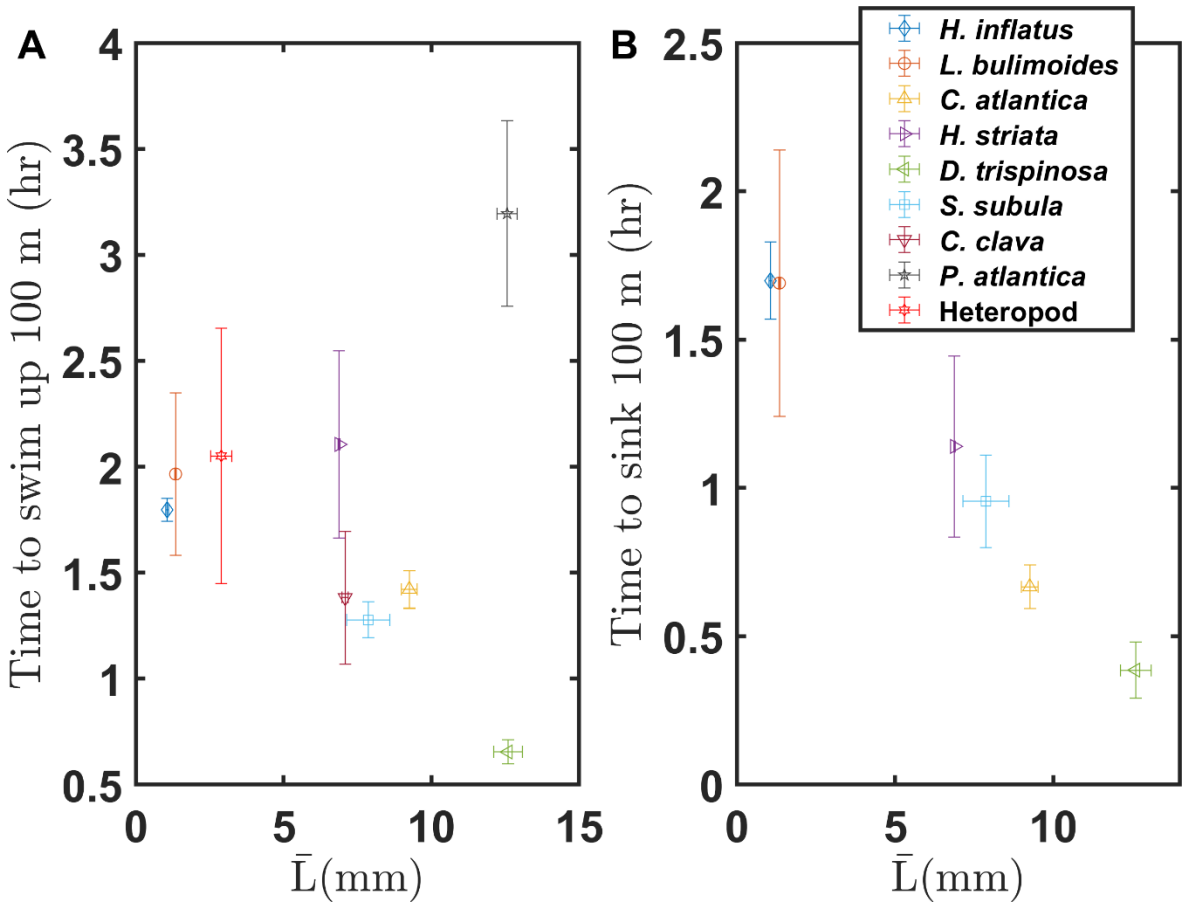

Figure 11: A) Upward and B) downward migration times over a distance of 100 m for various marine snail species, based on the mean swimming and sinking speeds measured here.

Table 1: Number of individual animals, videos, and video segments analyzed for each marine snail species

Order	Species	Minimum Number of Individual Species	Number of Videos	Number of Video Segments	Number of Videos Analyzed for Swimming	Number of Videos Analyzed for Sinking
Thecosome	*Heliconoides inflatus*	5	34	54	33	21
	Limacina bulimoides	2	4	7	4	3
	Cuvierina atlantica	3	28	34	21	13
	Hyalocylis striata	1	2	6	3	3
	Diacria trispinosa	3	8	11	8	3
	Creseis clava	1	4	4	4	0
	Styliola subula	2	7	15	10	5
Gymnosome	*Pneumoderma atlantica*	2	6	6	6	0
Heteropod	Atlantiid heteropod	2	2	2	2	0

Table 2: Comparison of morphological and swimming characteristics of various marine snail species from the current study and the literature. Values indicate mean and range (in parentheses).

Species	Reference	Body Length L (mm)	Wing Span L_f (mm)	Swimming Speed U (mm s^{-1})	Wingbeat Frequency f (Hz)	*Re*	Sinking Speed U_{sink} (mm s^{-1})	Re_{sink}
Clione limacina	Satterlie et al. (1985)	Up to 20	>5mm	100	1-3	Up to 1093	7-10	77-109
	Szymik and Satterlie (2011)	3-7	3.4-7.7	Tethered	1.1-3.2	NA	NA	NA
Clione antarctica	Borrell et al. (2005)	7-22	2.4-4.5	1-7	0.8-1.6	6-49	NA	NA
Limacina helicina	Chang and Yen (2012)	1-3.4	1-4	13-44	4.5-9.4	20-110	5-45	2-135
	Murphy et al. (2016)	1.6-2.0	2.1-2.9	15-26	4.3-4.7	19-42	NA	NA
Limacina helicina antarctica	Adhikari et al. (2016)	2.2	NA	21	2.9	29	NA	NA
	Mohaghar et. al. (2019)	1.5-4.5	5.0-9.0	14-30	1.9-3.0	13-55	NA	NA
Heliconoides inflatus	Current study	1.1 (0.9-1.2)	2.4 (2.3-2.4)	26 (12-55)	8.8 (6.6-11.1)	27 (12-66)	17 (13-22)	18 (12-29)
Limacina bulimoides		1.3 (1.3-1.4)	2.3 (2.1-2.7)	29 (18-40)	10.8 (10.1-11.5)	38 (22-51)	17 (16-19)	23 (22-25)
Cuvierina atlantica		9.3 (8.5-10.6)	9.1 (8.5-9.5)	33 (13-46)	5.5 (4.7-6.2)	294 (124-434)	45 (19-53)	411 (303-535)
Hyalocylis striata		6.9 (6.8-6.9)	6.6 (6.5-6.7)	22 (18-28)	7.9 (7.6-8.1)	146 (116-191)	25 (24-26)	169 (158-183)
Diacria trispinosa		12.6 (11.6-13.9)	12.3 (11.6-12.9)	84 (58-114)	6.1 (4.9-6.8)	1051 (680-1567)	86 (60-105)	1016 (830-1150)
Styliola subula		8.3 (3.6-8.7)	3.7 (1.6-4.0)	42 (17-63)	8.4 (6.1-10.5)	338 (148-505)	39 (22-52)	375 (348-417)
Creseis clava		7.1 (6.8-7.2)	3.8 (3.6-4.0)	38 (33-40)	12.0 (10.5-13.8)	262 (238-278)	NA	NA
Pneumoderma atlantica		12.6 (11.5-13.1)	5.1 (5.0-5.2)	18 (11-34)	4.0 (3.7-4.3)	224 (134-438)	NA	NA
Heteropod		2.9 (2.3-3.3)	1.7 (1.6-1.8)	29 (22-35)	9.5 (9.3-9.6)	84 (52-117)	NA	NA
Atlanta selvagensis	Karakas et al. (2018)	2.2	2.1	27	9.1	59	NA	NA

Table 3: MOCNESS distributions of species used in this study. The minimum (min) and maximum (max) depth (m) in which a large number of individuals of each group was observed in our image and molecular datasets. The depth of DVM was estimated from our data as well as from prior literature. Where inferred species names deviate from the molecular database due to recent changes in nomenclature are noted with a +. Information that was inferred from molecular datasets and applied to image or filming datasets are demarcated with a *.

Species	filmed	image min	image max	molecular min	molecular max	DVM extent	Literature source
Heliconoides inflatus	Y	0-50	250-400	Not identified in barcoding		~200 m	(Wormuth, 1981)
Limacina bulimoides	Y	0-50	150-250	Not identified in barcoding		~100 m	(Wormuth, 1981)
Cuvierina atlantica+	Y	0-50	300-400	0-50	300-400	~300 m	(Wormelle, 1962)
Hyalocylis striata	Y	50-200	50-200	0-50	50-200	~200 m	(Maas et al., 2012)
Diacria trispinosa	Y	50-200	300-400	50-200	300-400	~100 m	(Wormelle, 1962)
Styliola subula	Y	0-50	400-500	Not identified in barcoding		~250 m	(Wormuth, 1981)
Creseis clava	Y	0-50	50-200	0-50	50-200	~50	(Wormuth, 1981)
*Pneumoderma atlantica**	Y*	0-50*	0-50*	0-50	200-300	~100 m	
Gymnosomata sp.*	N	500-700*	500-700*	300-400	550-700	None	
Heteropoda	Y	0-50	400-500			multiple species	
Clio pyramidata	N	50-200	550-700	50-200	50-200	~400 m	(Wormuth, 1981)
Creseis conica+	N	0-50	50-200	Not identified in barcoding		~100 m	(Wormuth, 1981)
Diacria quadridentata	N	Not identified in MOCNESS		50-200	50-200	None	(Bé and Gilmer, 1977)
Limacina leuseruii	N	Not identified in MOCNESS		0-50	300-400	~200 m	(Wormuth, 1981)